Comparative analysis of vertebrates reveals that mouse primordial oocytes do not contain a Balbiani body

Laasya Dhandapani[1], Marion C. Salzer[1], Juan M. Duran[1], Gabriele Zaffagnini[1], Cristian De Guirior[3,4,5], Maria Angeles Martínez-Zamora[3,4,5], Elvan Böke[1,2*]

[1] Centre for Genomic Regulation (CRG), The Barcelona Institute of Science and Technology, Dr. Aiguader 88, Barcelona 08003, Spain;
[2] Universitat Pompeu Fabra (UPF), Barcelona, Spain
[3] Gynaecology Department, Institute Clinic of Gynaecology, Obstetrics and Neonatology, Hospital Clinic, Barcelona, Spain.
[4] Faculty of Medicine, University of Barcelona, Barcelona, Spain.
[5] Institut d'Investigacions Biomèdiques August Pi i Sunyer (IDIBAPS), Barcelona, Spain.

* Corresponding Author
Correspondence to Elvan Böke: elvan.boke@crg.eu
ORCID ID: 0000-0002-0760-7353
Mailing Address: Centre for Genomic Regulation (CRG), Dr. Aiguader 88, Edifici PRBB Barcelona 08003, Spain

ABSTRACT
Oocytes spend the majority of their lifetime in a primordial state. The cellular and molecular biology of primordial oocytes is largely unexplored; yet, it is necessary to study them to understand the mechanisms through which oocytes maintain cellular fitness for decades, and why they eventually fail with age. Here, we develop enabling methods for live-imaging-based comparative characterization of Xenopus, mouse and human primordial oocytes. We show that primordial oocytes in all three vertebrate species contain active mitochondria, Golgi and lysosomes. We further demonstrate that human and Xenopus oocytes have a Balbiani body characterized by a dense accumulation of mitochondria in their cytoplasm. However, despite previous reports, we did not find a Balbiani body in mouse oocytes. Instead, we demonstrate that what was previously used as a marker for the Balbiani body in mouse primordial oocytes is in fact a ring-shaped Golgi that is not functionally associated with oocyte dormancy. This study provides the first insights into the organization of the cytoplasm in mammalian primordial oocytes, and clarifies the relative advantages and limitations of choosing different model organisms for studying oocyte dormancy.

SUMMARY

Exploring the cytoplasmic features of human, mouse and frog early oocytes revealed that primordial oocytes have active organelles, and unlike human and Xenopus, mouse oocytes do not contain a Balbiani body.

INTRODUCTION

The earliest stage of a recognizable follicle in the ovary is the primordial follicle, which contains a primordial oocyte. The ovarian reserve consists of primordial oocytes, which are considered dormant as they do not grow nor divide (Reddy et al., 2010).

They can remain in the ovary for long periods of time, ranging from several weeks in mice to several decades in humans (Flurkey et al., 2007; Wallace and Kelsey, 2010). Each individual has a pool of thousands of primordial oocytes from which only a few are activated to grow at any given time. Upon sexual maturity, some of the growing oocytes mature to produce fertilizable eggs (Grive and Freiman, 2015; Rimon-Dahari et al., 2016).The most characteristic morphological feature of primordial oocytes of many species is the Balbiani body. The Balbiani body has also been referred to as the mitochondrial cloud in the literature (Guraya, 1979) and is a non-membrane bound super-organelle consisting mostly of mitochondria but also Golgi apparatus, endoplasmic reticulum (ER), other vesicles and RNA (Boke et al., 2016; Cox and Spradling, 2003; Hertig, 1968; Kloc et al., 2004). The Balbiani body is only present in early oocytes and dissociates upon oocyte activation. Therefore, it is closely associated with oocyte dormancy. In lower vertebrates, such as Xenopus and zebrafish, the Balbiani body is held together by an amyloid-like matrix formed by an intrinsically disordered protein (Boke et al.,2016; Krishnakumar et al., 2018), and is essential for the determination of the germline through inheritance of the germ plasm (Jamieson-Lucy and Mullins,2019; Kloc et al., 2004). Although the function of the Balbiani body in mammals remains elusive, it is proposed to protect mitochondria in the germline (Colnaghi et al., 2021; Jamieson-Lucy and Mullins, 2019; Kloc et al., 2004). This enigmatic super-organelle has been observed in, among others, humans (Hertig and Adams, 1967), chimpanzees (Barton and Hertig, 1972), cats (Amselgruber,1983), frogs (Al-Mukhtar and Webb, 1971; Boke et al., 2016) and zebrafish (Marlow and Mullins, 2008). Recent research has suggested that mouse primordial oocytes also contain a Balbiani body (Lei and Spradling, 2016; Pepling et al., 2007). Since virtually all of the organelles and cytoplasm of the zygote and hence, the new embryo, are derived from the oocyte, maintenance of oocyte health is imperative for producing healthy offspring (Cafe et al., 2021; Goodman et al., 2020; van der Reest et al., 2021). Although there is growing knowledge on how oocytes activate and interact with their somatic environment (Clarke, 2018; Handel et al., 2014; Li and Albertini, 2013; Matzuk et al., 2002), and how they segregate their chromosomes (Holubcová et al., 2015; Pfender et al., 2015), we know little about the cellular biology of dormant oocytes. Here, for the first time, we characterize and compare the cytoplasmic features of *Xenopus*, mouse and human primordial oocytes to study their cytoplasmic organization and organelle activity. We find that primordial oocytes of all three species contain active lysosomes, mitochondria and Golgi apparatus. In mouse oocytes, unlike human and *Xenopus*, mitochondria are not clustered within a Balbiani body. Furthermore, the conglomeration of Golgi stacks in mouse, which was previously used as a marker for the Balbiani body, is neither associated with RNA-binding proteins nor functionally connected with oocyte dormancy. We therefore provide strong evidence that mouse primordial oocytes, unlike human and *Xenopus*, do not contain a Balbiani body, thereby highlighting the similarities and differences between different model systems that are used to study oocyte dormancy.

RESULTS

Cytoplasmic organization is similar in *Xenopus* and human oocytes but different in mouse

Live-characterization of cells can reveal features that are lost after fixation such as organelle dynamics and activity. However, such studies do not yet exist for primordial oocytes. We began our studies by isolating follicle-enclosed oocytes from mouse, human, and *Xenopus* ovaries for live-imaging (Fig. S1A). The granulosa cells, which form the somatic component of the follicle, were used as internal controls to compare oocytes to somatic cells (Fig. 1A-C, G). We then probed the oocytes with fluorescent markers for mitochondria, lysosomes and the Golgi apparatus, and imaged them live to investigate the dynamics and activity of these organelles in the oocyte cytoplasm. We chose these three organelles for their fundamental roles in oocyte activation, growth and ageing (Cafe et al., 2021; Goodman et al., 2020; van der Reest et al., 2021). First, we imaged lysosomes with LysoTracker, which is a membrane permeable dye that preferentially accumulates in acidic, and thus active, lysosomes (Zhang, 1994). Previous studies suggested that lysosomes are inactive in early *C. elegans* oocytes (Bohnert and Kenyon, 2017; Samaddar et al., 2021). In contrast, lysosomes of all three vertebrate primordial oocytes accumulated LysoTracker (Fig. 1A, B, S1B). This labelling was lost upon incubation of oocytes with Bafilomycin A1, an inhibitor of lysosomal acidification (Bowman et al., 1988), confirming the specificity of the LysoTracker dye (Fig. S1B). The LysoTracker intensity was similar between somatic cells and primordial oocytes in all three species (Fig. 1A, B), as well as between primordial and growing oocytes (GVs) in mouse (Fig. S1C-D). Thus, we show for the first time that vertebrate primordial oocytes have acidic, active lysosomes distributed in their cytoplasm. Next, we used NBD C_6-Ceramide, a fluorescent sphingolipid derivative, to image the Golgi apparatus in live oocytes. NBD C_6-Ceramide is taken up by cells and transported to the Golgi apparatus, where it is metabolized and localized to the late Golgi cisternae (Lipsky and Pagano, 1985; Pagano et al.,1989). *Xenopus* and human oocytes displayed a distributed punctate pattern of Golgi in their cytoplasm, whereas NBD C_6-Ceramide showed a specific pattern previously described as a Golgi conglomerate in mouse oocytes (Fig. 1C, Movie S1) (Wischnitzer, 1970). The Golgi conglomerate, referred to as Golgi ring from here on, was not present in growing mouse oocytes (Fig. S1E-F). We found that the Golgi ring had polarized Golgi stacks as it contained cis- and trans-Golgi markers (GM130 and TGN46 respectively) and confirmed previous reports that it is associated with pericentrin (Lei and Spradling, 2016) (Fig. S1FH), similar to the Golgi apparatus in somatic cells (Klumperman, 2011). Thus, we conclude that the Golgi ring has structural features of a conventional Golgi apparatus. We asked whether the Golgi apparatus is capable of membrane trafficking, and thus, active in primordial oocytes. For this, we used Brefeldin A (BFA), one of the most specific compounds that acts on the Golgi apparatus to induce Golgi disassembly (Chardin and McCormick, 1999). BFA induces extensive tabulation of active Golgi apparatus cisternae and its ultimate fusion with ER membranes (Lippincott-Schwartz et al., 1990; Lippincott-Schwartz et al., 1989). Hence, an active Golgi apparatus is disassembled by BFA action, whereas a Golgi apparatus with impaired trafficking remains unaffected (Duran et al., 2012; Lippincott-Schwartz et al., 1990; Tan et al., 1992). We isolated primordial oocytes from mouse and *Xenopus* ovaries, treated them with BFA, and labelled their Golgi apparatus with NBD C_6-Ceramide for live-imaging. BFA treatment led to the dissociation of the Golgi apparatus

in mouse and *Xenopus* oocytes (Fig. 1D-F). We thus conclude that the Golgi apparatus in oocytes is capable of membrane trafficking and its structure is actively maintained. Finally, we imaged mitochondria in oocytes using tetramethylrhodamine ethyl ester (TMRE), a cell-permeant fluorescent dye that accumulates in active mitochondria dependent on mitochondrial membrane potential (Ehrenberg et al., 1988). All three vertebrate oocytes had detectable mitochondrial membrane potential as judged by TMRE labelling (Fig. 1G). Treatment of oocytes with CCCP, an ionophore which dissipates the mitochondrial membrane potential (Heytler, 1963), led to the loss of TMRE, confirming its specificity (Fig. S2A). In human and *Xenopus* oocytes, the majority of the mitochondria was present within the Balbiani body, as previously reported (Boke et al., 2016; Hertig and Adams, 1967) (Fig. 1G, S2B-C). Indeed, the center of the mitochondrial mass was mostly located inside the Balbiani body in human and *Xenopus* oocytes (Fig. S2B-C). In contrast, mitochondria of mouse oocytes were distributed throughout their cytoplasm (Fig. 1G, S2B-E) with the center of mitochondrial mass located inside their nucleus, confirming a more dispersed mitochondrial distribution (Fig. 1G, Fig. S2B-E). Finally, we compared mitochondrial distribution of *Xenopus,* mouse and human oocytes side-by-side using the same scale (Fig. S2F). This revealed that human and *Xenopus* oocytes have several micron wide spaces that are not occupied by mitochondria in their Balbiani bodies (Fig. S2F). Overall, we conclude that mitochondria are conglomerated in *Xenopus* and human primordial oocytes, whereas mouse oocytes have their mitochondria distributed in the cytoplasm. Primordial oocytes are almost exclusively obtained from neonatal mice in the recent literature (Shimamoto et al., 2019; Pepling et al., 2007; Morohaku et al., 2016; Castrillon et al., 2003; Eppig, et al., 2000). Since *Xenopus* and human oocytes in this study were isolated from young adults, we repeated our experiments using primordial oocytes obtained from young adult mice. We found that similar to newly formed primordial oocytes, young adult primordial oocytes also contain active organelles. Thus, primordial oocytes isolated from neonatal and young adult mice are similar regarding the activity of their organelles (Fig. S3A-C).Taken together, live-characterization revealed that primordial oocytes of all three vertebrates contain active lysosomes, Golgi apparatus and mitochondria.The cytoplasmic distribution of these organelles was similar in *Xenopus* and humans, but different in mouse (see schematic in Fig. 1H). We further confirmed this finding by immunostaining of fixed tissue sections (Fig. S1F-G, S3D-F).

Mitochondria in mouse primordial oocytes are not maintained within a proteinaceous matrix

Primordial oocytes of many species contain a Balbiani body, which is characterized by a dense accumulation of mitochondria adjacent to the nucleus (Kloc et al., 2004). The diffuse pattern of mitochondria in mouse oocytes prompted us to investigate whether mouse oocytes contain a Balbiani body. Previous studies have shown that the Balbiani body is held together by an amyloid-like matrix in *Xenopus* oocytes (Boke et al., 2016). To examine whether human and mouse oocytes contain amyloid-like assemblies in the form of a Balbiani body, we probed ovary sections with the aggresome dye, Proteostat, which is widely used in the literature to mark amyloid-like proteins (Olzscha et al., 2017; Tao et al., 2020; Usmani et al., 2014). Proteostat clearly marked the Balbiani bodies of *Xenopus* and human oocytes (Fig. 2A-B, S4A-B). In fact, the accumulation of the Proteostat dye was reminiscent of the mitochondrial distribution in these two species (Fig. 1G-H, 2A-B, S4A-B). On the other hand, we did not observe

a specific structure in the cytoplasm of mouse oocytes that would indicate a Balbiani body (Fig. 2C-D, S4A-B).

The Golgi ring is not a marker for the Balbiani body

Live-characterization and the Proteostat staining of tissue sections revealed that mouse primordial oocytes are different from human and *Xenopus* oocytes such that mouse oocytes do not have any mitochondrial conglomeration in the form of a Balbiani body (Fig. 1G, S2B-E, 2A-D, S4A, B). Our findings contrast with previous reports performed on thin mouse ovary sections, which suggested a degree of mitochondrial conglomeration around the Golgi ring, and the same reports used the Golgi ring as a marker for the Balbiani body (Lei and Spradling, 2016; Pepling et al., 2007). To clarify whether the Golgi ring is indeed associated with mitochondria, we labelled mitochondria and the Golgi ring in mouse primordial oocytes, and imaged them live. We confirmed our previous finding that mitochondria were distributed throughout the cytoplasm but were spatially excluded from the area of the Golgi ring (Fig. 3A, Movie S2). In fact, a Mitochondrial Exclusion Zone (MEZ) was present around the Golgi ring (Fig. 3A, arrowheads). We conclude that the Golgi ring is not associated with mitochondria in mouse primordial oocytes. It could be possible that mouse oocytes are unique in possessing a Balbiani body-*like* compartment that lacks mitochondria, but is comprised of the Golgi ring and RNA-binding proteins, held together by a protein matrix. We hypothesized that upon Golgi ring dissociation by BFA treatment, such a protein matrix/compartment would still occupy a space and would not allow the movement of large organelles, such as mitochondria, through (Fig. 3A, B). Therefore, the MEZ should be maintained under BFA treatment. To test this hypothesis, we disassembled the Golgi ring with BFA treatment as described above, and performed live-imaging of untreated and BFA-treated mouse primordial oocytes to follow their mitochondrial distribution (Fig. 3C). In untreated cells, which had an intact MEZ, mitochondria occupied 19% of the cytoplasm (Fig. 3C, D, S4C). Upon BFA treatment, the MEZ disappeared and mitochondria redistributed throughout the entire cytoplasm, almost doubling their occupancy to 35% of the cytoplasm (Fig. 3C-D, S4C). Similar results were obtained when we treated oocytes with Nocodazole, which causes the redistribution of the Golgi apparatus *via* a different mechanism than BFA (Cole et al., 1996; Turner and Tartakoff, 1989) (Fig. 3E-F). Thus, the redistribution of mitochondria upon Golgi ring disassembly suggests that mouse oocytes lack a proteinaceous matrix holding components of a presumed Balbiani body-*like* compartment (Fig. 3B). Finally, the Balbiani body has been implicated in the storage of RNAs complexed with RNA-binding proteins (RBPs) in organisms such as zebrafish and frogs that harbour a germ plasm (Jamieson-Lucy and Mullins, 2019; Kloc et al., 2004). However, because mammals do not contain a germ plasm, it was assumed that the mammalian Balbiani body would not contain RNAs (Kloc et al., 2004; Marlow, 2010). In contrast to this notion, two RBPs, namely RNGTT and RAP55, were suggested to localize to the Golgi ring, and then used as a marker for the mouse Balbiani body (Lei et al., 2020; Pepling et al., 2007). To test whether these RBPs indeed associated with the Golgi ring, we probed mouse oocytes for RNGTT and RAP55. RNGTT is a nuclear mRNA-capping enzyme that interacts with RNA Polymerase II (Galloway and Cowling, 2019), whereas RAP55 is an mRNA-binding protein that is localized to RNA granules (Yang et al., 2006) and ER-exit sites (Wilhelm et al., 2005). Neither of these proteins were detected in *Xenopus* Balbiani bodies (Boke et al., 2016). In mouse primordial oocytes, RNGTT only displayed nuclear localization, while RAP55 localized to DDX6-positive RNA

granules (Fig. 4A-D) that have been previously described during oocyte development (Kato et al., 2019). Neither of the two proteins displayed any particular accumulation within the Golgi ring (Fig.4A-C). Thus, we conclude that the Golgi ring does not associate with RNGTT or RAP55, and does not necessarily host any RNA-binding proteins. Since the Golgi ring does not associate with mitochondria, is not maintained within a proteinaceous matrix and does not co-localize with RNA-binding proteins, we conclude that the Golgi ring is not a marker for the Balbiani body in mouse primordial oocytes. Based on this, and together with our previous result showing that mouse oocytes lack mitochondrial conglomeration and an amyloid-like protein matrix, we conclude that mouse oocytes, unlike human and *Xenopus*, do not contain a Balbiani body.

The Golgi ring disassembly follows oocyte activation

We next asked whether the Golgi ring, which has been historically linked to oocyte dormancy (Lei and Spradling, 2016, Pepling et al., 2007, Jamieson-Lucy and Mullins, 2019), is required and thus functionally relevant for the maintenance of dormancy in mouse oocytes. To dissect the relationship between the presence of the Golgi ring and oocyte dormancy, we investigated whether primordial oocytes would activate and exit dormancy upon Golgi ring disassembly. The localization of the transcription factor FOXO3 serves as a dormancy marker in oocytes; it is nuclear in dormant oocytes, and is exported to the cytoplasm upon oocyte activation (Castrillon et al., 2003; Shimamoto et al., 2019). To monitor the relationship between the Golgi ring and FOXO3 in dormant and activated oocytes, in vitro culture of neonatal (P3) ovaries was performed. Ovaries were fixed immediately after extraction (t=0) or after 1 hour or 5 hours of in vitro culture and were processed for whole-mount imaging with GM130 and FOXO3 antibodies to check for the presence of the Golgi ring and the dormancy status of oocytes, respectively. As expected, at t=0, FOXO3 was nuclear in primordial oocytes and a Golgi ring was present in their cytoplasm (Fig. 5A), whereas growing oocytes showed cytoplasmic FOXO3, and a dissociating Golgi ring (Fig. 5A, C-D). After 1 hour of in vitro culture, oocytes started activating *en masse* as indicated by their cytoplasmic FOXO3 localisation as previously reported (Hayashi et al., 2020; Shimamoto et al., 2019) (Fig. 5B, D, S5A-B). After 5 hours of in vitro culture, nuclear FOXO3 localization remained low in all three replicates (Fig. 5B, D). The Golgi ring was present in the oocytes irrespective of FOXO3 localization (Fig. 5B-F, S5A-B), since more than 90% of oocytes still had a Golgi ring even after 5 hours of in vitro culture (Fig. 5B, E, S5A-B). This suggests that oocyte activation and the corresponding export of FOXO3 to the cytoplasm precedes the disassembly of the Golgi ring.

We next asked whether artificial disassembly of the Golgi ring would have any impact on oocyte activation. Disassembly of the Golgi ring was induced by treating whole ovaries with Brefeldin A during in vitro culture. One hour after Brefeldin A treatment, oocytes no longer had the Golgi ring (Fig. 5B, E, Movie S3, S4). Within each replicate, the percentage of oocytes with nuclear FOXO3 was comparable to untreated ovaries at the same time point (Fig. 5D). This suggests that artificial disassembly of the Golgi ring does not induce oocyte activation. Finally, ovaries were washed to remove Brefeldin A and cultured in fresh medium for an additional 4 hours. Surprisingly, almost all oocytes reformed their Golgi ring (Fig. 5B, E, S5A, Movie S5, S6) although many already had exited dormancy, judged by their cytoplasmic FOXO3 staining (Fig. 5B, D-F). Thus, we conclude that the Golgi ring formation is reversible, and not linked to

the dormancy status of the oocyte. Therefore, we conclude that the Golgi ring disassembly follows oocyte activation and does not have a causal function in this process. Moreover, the fact that activated oocytes can have a Golgi ring calls for caution to use the Golgi ring as a dormancy marker.

DISCUSSION

Here we performed the first live-characterization of primordial oocytes from three vertebrate species, that is, *Xenopus*, mouse and humans. This allowed us to address, for the first time, key questions of the cell biology of primordial oocytes, such as the activity and dynamics of individual organelles, their relationship with each other, and their association with dormancy. We showed that, unlike *Xenopus* and human, mouse oocytes do not have a Balbiani body or a Balbiani body-*like* compartment. This might seem surprising since humans and frogs are evolutionarily more distant to each other than mouse is to either species. However, a similar phenomenon has also been observed for the inheritance of the centrosome, which is similar between humans and *Xenopus*, but different in mice (Clift and Schuh, 2013; Schatten, 1994). We propose that this discrepancy could be explained by the different lengths of the reproductive lifespans of these animals. Oocytes are considered very long-lived cells. In particular, among the species we examined, human oocytes have the longest lifespan of the three, and can live up to 55 years (Wallace and Kelsey, 2010). *Xenopus laevis* oocytes can remain several years without growing in the ovaries (Callen et al., 1980; Keem et al., 1979), whereas mouse oocytes have the shortest lifespan, ranging from 8 to 14 months (Rugh, 1968). Since early embryogenesis depends on the integrity of the oocyte and its organelles, the oocyte cytoplasm has to remain intact throughout dormancy (Cafe et al., 2021; Goodman et al., 2020). We speculate that the Balbiani body serves to protect the quality of mitochondria and other organelles, and its necessity depends on the length of the reproductive lifespan of the species. This would be particularly true in those animals that do not require the Balbiani body to determine the future germ line in the form of germ plasm. Consistent with this prediction, the primordial oocytes of other mammals with short reproductive lifespans, such as rat, hamster, opossum and bandicoot, also lack an obvious Balbiani body in their cytoplasm, and rather present scattered mitochondria (Falconnier and Kress, 1992; Sotelo, 1959; Ullmann and Butcher, 1996; Weakley, 1966). Other mammalian systems with longer dormancy periods such as cows, dogs or pigs, or even non-mammalian species such as frogs or axolotl, may thus be more appropriate than mouse to study certain aspects of oocyte dormancy. We showed the Golgi ring, which was previously used as a marker for the Balbiani body in mouse oocytes (Lei and Spradling, 2016; Pepling et al., 2007) is not associated with oocyte dormancy. The Golgi ring has received attention in the field of oocyte dormancy likely due to its unconventional and apparently unique shape. However, although textbooks typically display the Golgi apparatus as a crescent-shaped ribbon (Klumperman, 2011), several different shapes of the Golgi apparatus are reported in different cell types (Kreft et al.,2010; Lu et al., 2001; Rao et al., 2018). In particular, a ring-shaped Golgi has also been reported in rat pituitary gonadotrophs and in HeLa cells depleted for a structural Golgi protein (Bassaganyas et al., 2019; Watanabe et al., 2012). We found that the Golgi ring in mouse oocytes contains stacked *cis*- and *trans*cisternae, associates with the centrosome as previously reported (Lei and Spradling, 2016), and is capable of active membrane trafficking. Therefore, the Golgi ring, despite having an unconventional shape, displays all the features of a conventional Golgi apparatus.

Finally, our data indicate that primordial oocytes in vertebrates, including humans, have metabolically active organelles. This is particularly interesting considering the need for the oocyte to keep its cytoplasm healthy for long periods of time. This suggests that oocytes require efficient mechanisms to prevent or reset intracellular damage caused by metabolic activity. Therefore, it will be of great interest for future research to study how vertebrate oocytes protect themselves from the by-products of metabolic activity during their longlasting dormancy.

MATERIALS AND METHODS

Ethics

All animals were sacrificed by accredited animal facility personnel before extraction of their ovaries. Ethical Committee permission to conduct the human oocytes aspect of this study was obtained from the Comité Étic d'Investigació Clínica CEIC-Parc de salut MAR (Barcelona) and Comité Ético de investigación Clínica CEIC-Hospital Clínic de Barcelona with approval number *HCB/2018/0497*. Written informed consent to participate was obtained from all participants prior to their inclusions in the study.

Animal Maintenance

Xenopus and mouse colonies used in this manuscript were housed in the Animal Facility of the Barcelona Biomedical Research Park (PRBB, Barcelona, Spain, EU). *Xenopus laevis* females were purchased from Nasco (NJ, USA). C57BL/6J mice were purchased from Charles River Laboratories and maintained under specific pathogen free conditions at 22°C, 12h light-dark cycles, and with access to food and water *ad libitum*. Female mice with aged between 3 days and 7 weeks were used for experiments.

Primordial oocyte isolation

Mouse:

Collagenase- or Liberase-mediated digestion: Primordial oocytes were isolated with a protocol modified from (Gosden, 1990). Briefly, the ovaries were digested in 1.5 mg ml^{-1} Collagenase IA (Sigma, C9891-1G) (ovaries from PND 3-4 mice) or in 0.2 mg ml- Liberase (Sigma, 5401119001) (ovaries from 5-6 weeks old mice) in medium M199 (Sigma Aldrich, 51322C) at 37ºC for 30 minutes on a benchtop shaker. After 30 minutes the solution was pipetted up and down to release individual follicles. The resulting suspension was neutralized with an equal volume of medium M199 (Gibco, 41550-020) containing 10% FBS (Gibco, 26140-087), 2.5mM Na-Pyruvate (Thermo, 11360070), 0.2% Na-DL-Lactate syrup (Sigma, L7900), 1x Penicillin-Streptomycin (Gibco, 15070-063) and 25 µg ml^{-1} DNaseIA (Sigma Aldrich CAS9003-08-9). The suspension was filtered through a 100 µm filter (Corning, CLS431752) to remove remaining ovary pieces. The solution was centrifuged at 300xg, 5 minutes, the supernatant decanted and pellet resuspended in fresh medium (as indicated above, without DNaseIA). The cells were transferred to a petri dish (33 X 10 mm, Corning, 351008) and placed in an incubator at 37ºC and 5% CO_2.

Trypsin mediated digestion: Primordial oocytes from neonatal (Postnatal day 3 or 4) mice ovaries were isolated with a protocol modified from (Eppig and Wigglesworth, *Biol. Reprod*., 2000). Briefly, the ovaries were digested in 0.05% Trypsin-EDTA (Gibco, 25300-054) with 0.02% DNase I (Sigma, DN25-100mg) at 37ºC for 30 minutes. The resulting suspension was neutralized with an equal volume of medium M199 (Gibco, 41550-020) containing 10% FBS (Gibco, 26140-087), 2.5 mM Na-Pyruvate (Thermo, 11360070), 0.2% Na-DL-Lactate syrup (Sigma, L7900), 1x Penicillin-Streptomycin (Gibco, 15070-063) and centrifuged at 850 rpm for 3 minutes. The supernatant was decanted, and cells were transferred to a petri dish (33 X 10 mm, Corning, 351008) and placed in an incubator at 37ºC and 5% CO_2. All mouse oocyte imaging experiments were conducted in the medium mentioned above.

Human: Donations were provided by the gynaecology service of Hospital Clinic Barcelona, from women aged 19 to 34 undergoing ovarian surgery**.** Women fulfilling the inclusion criteria undergoing ovarian surgery were asked to participate in the study. Informed consent was obtained from all of them. Inclusion criteria: Age between 18 to 35, fertile (assessed by un-induced menstrual cycles or presence of antral follicles identified by ultrasound examination), presence of at least one ovary, signed informed consent. Exclusion criteria**:** women with menopause, endometriosis, or who underwent bilateral oophorectomy. All oocytes incorporated in this study were from women free of disease affecting the reproductive system. Donated ovarian cortex samples were transported in Leibovitz medium (Gibco, 21083- 027) containing 3 mg ml^{-1} BSA (Heat Shock Fraction, Sigma A7906) and quickly cut into 3 mm cubic pieces. Ovary pieces were transferred to DMEM containing 25 mM HEPES (Gibco, 21063-029) and 2 mg ml^{-1} collagenase type III (Worthington Biochemical Corporation, LS004183) and were left for digestion in a 37°C incubator with a 5% CO2 atmosphere for 2 hours, with occasional swirling of the petri dishes (100 X 20 mm, Corning 353003). After 2 hours, the resulting suspension containing individual cells was separated from tissue fragments by sedimentation in a 50 ml falcon tube and collagenase III was neutralized adding a 1:1 amount of DMEM/F12 medium (Gibco, 11330-032) containing 15 mM HEPES and 10% FCS (Gibco, 10270106). Individual human follicles are several magnitudes larger in volume and thus heavier than other single cells in the suspension. Incorporating this feature of follicles into the isolation protocol vastly improved the efficiency of isolation: After transferring the above supernatant to petri dishes, oocytes sedimented to the bottom within 15 seconds. We then removed the top layers of the single cell suspension by suction to have a primordial follicle enriched petri dish, mostly cleaned from other cells of the ovary. Follicles were picked manually under a dissecting microscope with a p10 pipette and transferred to a tissue culture dish. We obtain 60 to 180 primordial follicles from each of our ovary preparations. Leftover fragments of tissue were treated again for 2 hours with DMEM containing 25 mM HEPES and collagenase III for further 2 hours and follicles were picked as before. All human oocyte imaging experiments were conducted in the medium mentioned above.

Frog: Oocytes were isolated from young adult *Xenopus* (aged 3 to 5 years) ovaries according to the protocol described in (Boke et al., 2016). Briefly, ovaries were digested using 2 mg ml^{-1} Collagenase IA (Sigma, C9891-1G) in MMR by gentle rocking until dissociated oocytes were visible, for 30 to 45 minutes. The resulting mix was passed through two sets of filter meshes, the first with 297 µm mesh size and the second with 250 µm mesh size (Spectra/Mesh, 146424, 146426). All washes were performed in MMR. Oocytes which passed through the 250 micron mesh were washed once more with MMR and transferred to OCM (Boke et al., 2016; Mir and Heasman, 2008). All frog oocyte imaging experiments were conducted in OCM at room temperature and atmospheric air.

Germinal vesicle oocyte isolation from mouse

Ovaries of 6-week-old mice were dissected in M2 medium (Sigma, M7167) to remove the fat pad and oviducts attached to the ovaries. The ovaries were punctured using an insulin needle to release germinal vesicle (GV) stage oocytes. The oocytes were collected with an oocyte manipulation pipette and transferred to a new dish containing M2 medium (Sigma, M7167) + 400µM dbcAMP (Sigma, D0627) and incubated at 37ºC, atmospheric air.

Oocyte classification

Oocytes are classified according to their size and morphology in both mammalian and frog reproduction fields (Dumont, 1972; Gougeon, 1986; Pedersen and Peters, 1968; Westergaard et al., 2007). *Xenopus* oocytes were classified according to (Dumont, 1972). The average early stage I *Xenopus laevis* oocyte was 200 µm in diameter and surrounded by a single layer somatic granulosa cells. Primordial oocytes in humans were approximately 30 µm in diameter and surrounded by a single layer of flattened pre-granulosa cells (Gougeon, 1986; Westergaard et al., 2007). Primordial oocytes in mice were classified according to their size

(Pedersen and Peters, 1968) and were 15-17 µm in diameter. They were also surrounded by a single layer of flattened pregranulosa cells. For cartoon representations of the oocytes and flattened pre-granulosa cells, see Fig. 1H.

In vitro ovary culture

Neonatal ovaries were dissected, cleaned of adjoining tissue in M2 medium (Sigma, M7167) and placed on Millicell hanging cell culture inserts (Merck, MCSP24H48) in a 24 well plate (Greiner bio-one, 662160). 500 µl of DMEM/F12 medium (Gibco, 31331-028) supplemented with 10% FBS (Gibco, 26140-087) and 1x Penicillin-Streptomycin (Gibco, 15070-063) was introduced into each well such that a thin layer of liquid was present above the ovary. The ovaries were cultured for indicated times in an incubator at 37ºC and 5% CO_2.

Fluorescent Dyes

TMRE: Tetramethylrhodamine ethyl ester, Percholorate (TMRE) (Thermo, T669) was added to oocytes of all species at a final concentration of 500 nM and incubated for 30 minutes. Oocytes were washed and plated on 35mm glass bottom MatTek (MatTek Corporation, P35G 1.5-20-C) dishes in fresh medium.

LysoTracker: LysoTracker Deep Red (Thermo, L12492) was added to the oocytes of all 3 species at a final concentration of 50 nM and incubated for 30 minutes. Oocytes were washed and plated on glass bottom MatTek dishes in fresh medium.

NBD C_6-Ceramide: Human and mouse oocytes (including GV oocytes obtained from mouse) were incubated in medium containing NBD C_6-Ceramide (Thermo, N22651) to a final concentration of 5 µM for 30 minutes (3 µm only in the case of mouse oocytes obtained through 'Trypsin mediated digestion' as mentioned in Materials and Methods) at 37ºC, and 5% CO_2. The oocytes were then washed and plated on MatTek dishes in fresh medium. *Xenopus* oocytes were incubated with 5 µM NBD C_6-Ceramide at 4ºC for 30 minutes, washed and incubated at 18ºC for a further 30 minutes.

NBD C_6-Ceramide + MitoTracker: Mouse oocytes were incubated in medium containing 3 µM NBD C_6-Ceramide (Thermo, N22651) and 100 nM MitoTracker Deep Red FM (Thermo, M22426) to visualize the Golgi apparatus and mitochondria. After 30 minutes, the oocytes were washed, plated on MatTek dishes and imaged live.

Proteostat: Ovaries were dissected from *Xenopus*, neonatal (PND4) and adult mice (8 weeks old). Human ovarian cortex pieces were donated by patients. The tissues were fixed in 4% Paraformaldehyde, embedded in paraffin and cut into 5µm sections. Staining was performed adapting the manufacturer's instructions (Proteostat Aggresome Detection Kit, ENZ-51035-K100). Formalin fixed paraffin embedded tissue sections from neonatal and adult mice, *Xenopus* and human were deparaffinized, permeabilized for 30 minutes on ice as recommended by the manufacturer. Proteostat was added at 1:2000 final concentration and Hoechst at 1:1000 for 30 minutes in the dark. The slides washed, mounted and imaged on Leica TCS SPE microscope using 63x oil immersion objective (N.A: 1.40, Leica, 506350). The images were analysed using Fiji/ImageJ. For Fig. S5A, top 10% fluorescent intensity thresholding masks were applied in Fiji to the Proteostat signal in the oocytes of all 3 species.

Drug Treatments

CCCP treatment: Isolated oocytes were incubated in culture medium containing carbonyl cyanide m-chlorophenyl hydrazine (Abcam, ab141229) at a final concentration of 30 µM for 15 minutes, followed by TMRE addition.

Bafilomycin A1 treatment: Isolated *Xenopus* and mouse oocytes were incubated in a droplet of medium containing Bafilomycin A1 (Abcam, ab120497) at a final concentration of 500 nM (*Xenopus)* or 100 nM (mouse) for 1 hour, followed by addition of LysoTracker Deep Red as described above.

Brefeldin A treatment: Primordial oocytes isolated from neonatal or young adult (5-6 weeks old) mice were incubated in culture media containing Brefeldin A (BFA) (Abcam, ab120299) at a final concentration of 10 µM for 30 minutes. Whole P3 ovaries were placed on Millicell hanging cell culture inserts (Merck, MCSP24H48) in 500µL medium with 10 µM Brefeldin A for 1 hour in a 24 well-plate (Greiner bio-one, 662160). The ovaries were then either fixed in 4% PFA and processed for whole-mount immunostaining or transferred for 4 hours to BFA free medium for 4 hours before fixing them. *Xenopus* oocytes were isolated and incubated in OCM containing a final concentration of 10 µM Brefeldin A for 30 minutes. Then the BFA was washed and oocytes were incubated with NBD C_6-Ceramide as described above.

Nocodazole treatment: Isolated oocytes were incubated in culture media containing Nocodazole (Sigma, M1404) at a final concentration of 5 µM for 45 minutes to 1 hour. The oocytes were then incubated in medium containing NBD C_6-Ceramide (Thermo, N22651) and MitoTracker Deep Red FM (Thermo, M22426) to visualize the Golgi apparatus and mitochondria.

Live-cell imaging

Mouse and human oocytes were imaged in their respective culture medium in a Leica TCS SP5 STED microscope using a 63x water immersion objective (N.A 1.20, Leica, 506279) with an incubation chamber maintained at 37ºC and 5% CO_2. Frog oocytes were imaged in OCM at room temperature and atmospheric air in a Leica TCS SP8 microscope using a 40x water immersion objective (N.A 1.10, Leica, 506357). All images were acquired using the Leica Application Suite X (LAS X) software. The images were analysed using Fiji/ ImageJ.

Immunohistochemistry

Sample preparation – mouse: Neonatal (P3 or P4) ovaries were dissected in M2 medium (Sigma, M7167) to remove the surrounding tissue and fixed in 4% PFA in PBS at 4ºC for 3 hours. For preparing frozen sections, ovaries were transferred to 30% Sucrose in PBS overnight at 4ºC. The next day, ovaries were placed in OCT medium within a mould and 20 µm-thick sections were cut using a microtome and transferred onto glass slides. Alternatively, ovaries were embedded in paraffin after fixation and 5µm-thick sections were cut and transferred onto glass slides.

Sample preparation – human: Fragments of human ovary of about 3x3mm were cut from the cortex and fixed in 4% PFA in 100mM phosphate buffer pH 7.5 for 4 hours at room temperature. Samples were then embedded in paraffin and 5 µm-thick sections were cut and transferred onto glass slides.

Sample preparation – *Xenopus*: Fragments of *Xenopus* ovary of about 1x1 cm were cut from freshly extracted ovaries and fixed in 4% PFA in PBS at 4ºC overnight. The next day, the ovary pieces were embedded in paraffin and 5 µm-thick sections were cut and transferred onto glass slides.

Immunostaining: Paraffin-embedded sections were deparaffinized, boiled in 10 mM Sodium Citrate pH 6.0 and directly blocked in blocking buffer (PBS containing 3% BSA, 2% Normal Goat Serum and 0.05% Tween-20) for 1 hour. Frozen sections were equilibrated at room temperature for 10 minutes and washed in PBS for 15 minutes in Coplin jars. The sections were then permeabilized (PBS containing 0.2% Triton X100 and 0.1% Tween-20) for 30 minutes and blocked in blocking buffer for 1 hour before proceeding with antibody incubation.

Isolated primordial follicles were fixed in 2% PFA for 15 minutes at room temperature in an Eppendorf tube, permeabilized and blocked with the respective buffers mentioned above. The primary antibodies were diluted in blocking solution. Follicles and section were incubated with primary antibodies overnight at 4ºC. The primary antibodies were against GM130 (1:100, BD, 610822), TGN46 (1:100, Abcam, ab16059), Pericentrin (1:100, Abcam, ab4448), RNGTT (1:100, Abcam ab201046) and RAP55 (1:100, Abcam, ab221041), ATP5A (1:100, abcam, ab14748), LAMP1 (1:100, Abcam ab24170), LAMP1 (1:100, ab25245), Mannosidase II (1:100, Merck AB3712), DDX4 (1:100, Abcam ab27591) and DDX4 (1:100, Abcam ab13840). Secondary antibodies goat anti-mouse Alexa488 (1:1000, Invitrogen, A32723), goat anti-rabbit Alexa647 (1:1000, Invitrogen, A21245), goat anti-mouse Alexa 555 (1:1000, Abcam ab150114) or goat anti-rat Alexa546 (1:1000, Invitrogen, A-11081) were diluted in blocking solution. Samples were imaged in a droplet of mounting medium containing DAPI (Abcam, ab104139). Imaging was carried out in Leica TCS SP5 or Leica TCS SP8 microscopes using 63x oil immersion objectives (N.A 1.40, Leica 15506350) in the case of sections or 63x water immersion objective (N.A 1.20, Leica, 506346) in the case of isolated follicles. The images were analysed using Fiji/ ImageJ.

Whole-mount immunostaining

Whole-mount immunostaining was performed according to (Rinaldi et al., 2018). The ovaries were incubated with primary antibodies (rabbit anti-FOXO3 [Cell Signal, 2497S], mouse anti GM130 [BD, 610822], rabbit anti-RAP55 [Abcam, ab221041] and mouse anti-DDX6 [SCBT, sc-376433]) in the ratio of 1:100 in blocking solution for 48 hours. After an overnight wash, ovaries were incubated with 1:1000 of secondary antibodies goat anti-mouse Alexa488 (1:1000, Invitrogen, A32723) and goat anti-rabbit Alexa647 (1:1000, Invitrogen, A21245) in blocking solution for 48 hours. The ovaries were washed overnight with wash buffer, followed by an incubation with 50 µg/ml DAPI in wash buffer for 8 hours and another overnight wash. The ovaries were imaged in a droplet of PBS on a MatTek dish using a Leica TCS SP8 microscope with 20x air (N.A 0.70, Leica, 11506166) or 40x oil immersion (11506358, Leica, N.A 1.30) objective. The images were analysed using Fiji/ ImageJ.

FOXO3 localization and GM130 ring quantification

Z-stacks of 20 µm were made by imaging whole-mount ovaries at 1 µm sections. The oocytes were marked by creating ROIs in Fiji ROI Manager based on FOXO3, GM130 and DAPI staining. FOXO3 staining was assessed manually as nuclear or cytoplasmic and the number of oocytes in each case was recorded. Similarly, the presence of the Golgi ring as seen by GM130 staining was counted in these oocytes. Nuclear FOXO3 and the presence of the Golgi ring were quantified for ovaries cultured in vitro for 0, 1 and 5 hours in the absence of BFA (untreated), treated with BFA for 1 hour and treated with BFA for 1 hour followed by a 4-hour washout. The corresponding values at each time point were plotted by GraphPad software.

Mitochondrial occupancy calculation

Oocytes isolated from neonatal (P3 or P4) mice were treated with Brefeldin A, incubated with 3 µM NBD C_6-ceramide and 100nM MitoTracker Deep Red FM (Thermo, M22426) to visualize the Golgi apparatus and mitochondria. After 30 minutes, the oocytes were washed, plated on MatTek dishes and imaged live. The area of the oocyte cytoplasm was determined by subtracting the area of the nucleus from the whole area of the oocytes (Fig. S4C). A mask was created to select mitochondria using the threshold function in Fiji/ImageJ. The mitochondrial occupancy was then calculated as

$$Mitochondrial\ occupancy\ (\%) = \frac{area\ occupied\ by\ mitochondria}{area\ of\ oocyte\ cytoplasm} \times 100$$

The MEZ calculations were performed on the equatorial sections of the oocytes. Significance of the difference in mitochondrial occupancy in untreated versus BFA treated oocytes was

assessed using student's t test. Similar quantifications were performed after oocytes were treated with nocodazole as mentioned under the section 'Drug treatments'.

Mitochondrial Center of Mass Calculation
Oocytes isolated from neonatal mice (PD4) or young adult *Xenopus* and human ovaries were incubated with TMRE and imaged as described. The mitochondrial mass was demarcated manually as shown in Fig. S2B and the center of mass function of Fiji was applied to it. The coordinates of the mitochondrial center of mass were used to determine its location as indicated in Fig. S2C (see schematic).

Lysotracker Intensity measurement
Lysosomes on same Z-sections were used to avoid z-depth-related fluorescent intensity loss. After background subtraction, images were duplicated, and subjected to a threshold to detect lysosomes. A mask was created from the thresholded image, which was applied to the original image to detect all lysosomes (Fig. S1C). Fluorescent intensities of lysosomal puncta were measured individually and plotted in Fig. 1B.

ACKNOWLEDGEMENTS
We thank Nicholas Stroustrup and Vivek Malhotra for critical reading of the manuscript; Ishier Raote for his insightful comments; the PRBB Animal Facility personnel for their continued support; the Histology Facility (Alexis Rafols Mitjans); and the Advanced Light Microscopy team (especially Timo Zimmerman). We acknowledge support of the Spanish Ministry of Science and Innovation to the EMBL partnership, the Centro de Excelencia Severo Ochoa and the CERCA Programme/Generalitat de Catalunya.

AUTHOR CONTRIBUTIONS
E.B. conceived and designed the project, performed *Xenopus* experiments and helped perform human oocyte isolation and imaging experiments with J.M.D. All mouse experiments were performed by L.D. except for Fig. 2, Fig. S4C and Fig. S5 (L.D. together with G.Z.). M.C.S. helped devise oocyte isolation protocols and ovary isolations. C.D.G and M.A.M.Z. informed patients and supervised the collection of human ovarian cortex from surgeries. The manuscript was written by L.D., M.C.S., and E.B. with input from all authors.

Funding
This study was supported by a European Research Council Starting Grant (ERC-StG-2017-759107) and the Ministerio de Ciencia e Innovación (MINECO - BFU2017-89373-P and PID2020-115127GB-I00 to E.B.). G.Z. acknowledges funding from the European Union's Horizon 2020 research and innovation programme under the Marie Skłodowska-Curie grant agreement No 754422. M.S. is supported by a Juan de la Cierva-Formación fellowship from the Ministerio de Ciencia e Innovación (FJC2019-041607-I; AEI; 10.13039/ 501100011033).

REFERENCES

Al-Mukhtar, K.A., and A.C. Webb. 1971. An ultrastructural study of primordial germ cells, oogonia and early oocytes in Xenopus laevis. *Development*. 26:195-217.

Amselgruber, V.W. 1983. Licht-und elektronenmikroskopische Untersuchungen zur Oogenese der Katze (Felis catus). *Anatomia, Histologia, Embryologia*. 12:193-229.

Banani, S.F., H.O. Lee, A.A. Hyman, and M.K. Rosen. 2017. Biomolecular condensates: organizers of cellular biochemistry. *Nature reviews Molecular cell biology*. 18:285-298.

Barton, B.R., and A.T. Hertig. 1972. Ultrastructure of annulate lamellae in primary oocytes of chimpanzees (Pan troglodytes). *Biology of reproduction*. 6:98-108.

Bassaganyas, L., S.J. Popa, M. Horlbeck, C. Puri, S.E. Stewart, F. Campelo, A. Ashok, C.M. Butnaru, N. Brouwers, and K. Heydari. 2019. New factors for protein transport identified by a genome-wide CRISPRi screen in mammalian cells. *Journal of Cell Biology*. 218:3861-3879.

Bohnert, K.A., and C. Kenyon. 2017. A lysosomal switch triggers proteostasis renewal in the immortal C. elegans germ lineage. *Nature*. 551:629-633.

Boke, E., M. Ruer, M. Wühr, M. Coughlin, R. Lemaitre, S.P. Gygi, S. Alberti, D. Drechsel, A.A. Hyman, and T.J. Mitchison. 2016. Amyloid-like selfassembly of a cellular compartment. *Cell*. 166:637-650.

Bowman, E.J., A. Siebers, and K. Altendorf. 1988. Bafilomycins: a class of inhibitors of membrane ATPases from microorganisms, animal cells, and plant cells. *Proceedings of the National Academy of Sciences*. 85:7972-7976.

Cafe, S.L., B. Nixon, H. Ecroyd, J.H. Martin, D.A. Skerrett-Byrne, and E.G. Bromfield. 2021. Proteostasis in the Male and Female Germline: A New Outlook on the Maintenance of Reproductive Health. *Frontiers in cell and developmental biology*. 9:870.

Callen, J., N. Dennebouy, and J. Mounolou. 1980. Kinetic analysis of entire oogenesis in Xenopus laevis. *Development, Growth & Differentiation*. 22:831-840.

Castrillon, D.H., L. Miao, R. Kollipara, J.W. Horner, and R.A. DePinho. 2003. Suppression of ovarian follicle activation in mice by the transcription factor Foxo3a. *Science*. 301:215-218.

Chardin, P., and F. McCormick. 1999. Brefeldin A: the advantage of being uncompetitive. *Cell*. 97:153-155.

Clarke, H.J. 2018. Regulation of germ cell development by intercellular signaling in the mammalian ovarian follicle. *Wiley Interdisciplinary Reviews: Developmental Biology*. 7:e294.

Clift, D., and M. Schuh. 2013. Restarting life: fertilization and the transition from meiosis to mitosis. *Nature reviews Molecular cell biology*. 14:549-562.

Cole, N.B., N. Sciaky, A. Marotta, J. Song, and J. Lippincott-Schwartz. 1996. Golgi dispersal during microtubule disruption: regeneration of Golgi stacks at peripheral endoplasmic reticulum exit sites. *Molecular biology of the cell*. 7:631-650.

Colnaghi, M., A. Pomiankowski, and N. Lane. 2021. The need for high-quality oocyte mitochondria at extreme ploidy dictates mammalian germline development. *Elife*. 10:e69344.

Cox, R.T., and A.C. Spradling. 2003. A Balbiani body and the fusome mediate mitochondrial inheritance during Drosophila oogenesis. *Development*. 130:1579-1590.
Dumont, J.N. 1972. Oogenesis in Xenopus laevis (Daudin). I. Stages of oocyte development in laboratory maintained animals. *Journal of morphology*. 136:153-179.
Duran, J.M., F. Campelo, J. Van Galen, T. Sachsenheimer, J. Sot, M.V. Egorov, C. Rentero, C. Enrich, R.S. Polishchuk, and F.M. Goñi. 2012. Sphingomyelin organization is required for vesicle biogenesis at the Golgi complex. *The EMBO journal*. 31:4535-4546.
Ehrenberg, B., V. Montana, M. Wei, J. Wuskell, and L. Loew. 1988. Membrane potential can be determined in individual cells from the nernstian distribution of cationic dyes. *Biophysical journal*. 53:785-794.
Falconnier, C., and A. Kress. 1992. Ultrastructural aspects of oocyte growth in the marsupial Monodelphis domestica (grey short-tailed opossum). *Journal of anatomy*. 181:481.
Flurkey, K., J.M. Currer, and D. Harrison. 2007. Mouse models in aging research. *In* The mouse in biomedical research. Elsevier. 637-672.
Galloway, A., and V.H. Cowling. 2019. mRNA cap regulation in mammalian cell function and fate. *Biochimica et Biophysica Acta (BBA)-Gene Regulatory Mechanisms*. 1862:270-279.
Goodman, J.S., G.A. King, and E. Ünal. 2020. Cellular quality control during gametogenesis. *Experimental Cell Research*:112247.
Gosden, R. 1990. Restitution of fertility in sterilized mice by transferring primordial ovarian follicles. *Human Reproduction*. 5:117-122.
Gougeon, A. 1986. Dynamics of follicular growth in the human: a model from preliminary results. *Human reproduction*. 1:81-87.
Grive, K.J., and R.N. Freiman. 2015. The developmental origins of the mammalian ovarian reserve. *Development*. 142:2554-2563.
Guraya, S.S. 1979. Recent advances in the morphology, cytochemistry, and function of Balbiani's vitelline body in animal oocytes. *International review of cytology*. 59:249-321.
Handel, M.A., J.J. Eppig, and J.C. Schimenti. 2014. Applying “gold standards” to in-vitro-derived germ cells. *Cell*. 157:1257-1261.
Hayashi, K., S. Shimamoto, and G. Nagamatsu. 2020. Environmental factors for establishment of the dormant state in oocytes. *Development, Growth & Differentiation*. 62:150-157.
Hayes, M.H., and D.L. Weeks. 2016. Amyloids assemble as part of recognizable structures during oogenesis in Xenopus. *Biology open*. 5:801-806.
Hertig, A.T. 1968. The primary human oocyte: some observations on the fine structure of Balbiani's vitelline body and the origin of the annulate lamellae. *Developmental Dynamics*. 122:107-137.
Hertig, A.T., and E.C. Adams. 1967. Studies on the human oocyte and its follicle. *The Journal of Cell Biology*. 34:647-675.
Heytler, P. 1963. Uncoupling of oxidative phosphorylation by carbonyl cyanide phenylhydrazones. I. Some characteristics of m-CI-CCP action on mitochondria and chloroplasts. *Biochemistry*. 2:357-361.
Holubcová, Z., M. Blayney, K. Elder, and M. Schuh. 2015. Error-prone chromosome-mediated spindle assembly favors chromosome

segregation defects in human oocytes. *Science*. 348:1143-1147.
Jamieson-Lucy, A., and M.C. Mullins. 2019. The vertebrate Balbiani body, germ plasm, and oocyte polarity. *In* Current topics in developmental biology. Vol. 135. Elsevier. 1-34.
Kato, Y., T. Iwamori, Y. Ninomiya, T. Kohda, J. Miyashita, M. Sato, and Y. Saga. 2019. ELAVL2-directed RNA regulatory network drives the formation of quiescent primordial follicles. *EMBO reports*. 20:e48251.
Keem, K., L.D. Smith, R.A. Wallace, and D. Wolf. 1979. Growth rate of oocytes in laboratory-maintained Xenopus laevis. *Gamete Research*. 2:125-135.
Kloc, M., S. Bilinski, and L.D. Etkin. 2004. The Balbiani body and germ cell determinants: 150 years later. *In* Current topics in developmental biology. Vol. 59. Elsevier. 1-36.
Klumperman, J. 2011. Architecture of the mammalian Golgi. *Cold Spring Harbor perspectives in biology*. 3:a005181.
Kreft, M.E., D. Di Giandomenico, G.V. Beznoussenko, N. Resnik, A.A. Mironov, and K. Jezernik. 2010. Golgi apparatus fragmentation as a mechanism responsible for uniform delivery of uroplakins to the apical plasma membrane of uroepithelial cells. *Biology of the Cell*. 102:593-607.
Krishnakumar, P., S. Riemer, R. Perera, T. Lingner, A. Goloborodko, H. Khalifa, F. Bontems, F. Kaufholz, M.A. El-Brolosy, and R. Dosch. 2018. Functional equivalence of germ plasm organizers. *PLoS genetics*. 14:e1007696.
Lei, L., K. Ikami, H. Abbott, and S. Jin. 2020. The mouse Balbiani body maintains primordial follicle quiescence via RNA storage. *bioRxiv*.
Lei, L., and A.C. Spradling. 2016. Mouse oocytes differentiate through organelle enrichment from sister cyst germ cells. *Science*. 352:95-99.
Li, R., and D.F. Albertini. 2013. The road to maturation: somatic cell interaction and self-organization of the mammalian oocyte. *Nature reviews Molecular cell biology*. 14:141-152.
Lippincott-Schwartz, J., J.G. Donaldson, A. Schweizer, E.G. Berger, H.-P. Hauri, L.C. Yuan, and R.D. Klausner. 1990. Microtubule-dependent retrograde transport of proteins into the ER in the presence of brefeldin A suggests an ER recycling pathway. *Cell*. 60:821-836.
Lippincott-Schwartz, J., L.C. Yuan, J.S. Bonifacino, and R.D. Klausner. 1989. Rapid redistribution of Golgi proteins into the ER in cells treated with brefeldin A: evidence for membrane cycling from Golgi to ER. *Cell*. 56:801-813.
Lipsky, N.G., and R.E. Pagano. 1985. A vital stain for the Golgi apparatus. *Science*. 228:745-747.
Lu, Z., D. Joseph, E. Bugnard, K.J. Zaal, and E. Ralston. 2001. Golgi complex reorganization during muscle differentiation: visualization in living cells and mechanism. *Molecular Biology of the Cell*. 12:795-808.
Marlow, F.L. 2010. Maternal control of development in vertebrates. *In* Colloquium Series on Developmental Biology. Vol. 1. Morgan & Claypool Life Sciences. 1-196.
Marlow, F.L., and M.C. Mullins. 2008. Bucky ball functions in Balbiani body assembly and animal–vegetal polarity in the oocyte and follicle cell layer in zebrafish. *Developmental biology*. 321:40-50.
Matzuk, M.M., K.H. Burns, M.M. Viveiros, and J.J. Eppig. 2002. Intercellular communication in the mammalian ovary: oocytes carry the conversation.

Science. 296:2178-2180.
Mir, A., and J. Heasman. 2008. How the mother can help: studying maternal Wnt signaling by anti-sense-mediated depletion of maternal mRNAs and the host transfer technique. *In* Wnt Signaling. Springer. 417-429.
Olzscha, H., O. Fedorov, B.M. Kessler, S. Knapp, and N.B. La Thangue. 2017. CBP/p300 bromodomains regulate amyloid-like protein aggregation upon aberrant lysine acetylation. *Cell chemical biology*. 24:9-23.
Pagano, R.E., M.A. Sepanski, and O.C. Martin. 1989. Molecular trapping of a fluorescent ceramide analogue at the Golgi apparatus of fixed cells: interaction with endogenous lipids provides a trans-Golgi marker for both light and electron microscopy. *The Journal of Cell Biology*. 109:2067-2079.
Pedersen, T., and H. Peters. 1968. Proposal for a classification of oocytes and follicles in the mouse ovary. *Reproduction*. 17:555-557.
Pepling, M.E., J.E. Wilhelm, A.L. O'Hara, G.W. Gephardt, and A.C. Spradling. 2007. Mouse oocytes within germ cell cysts and primordial follicles contain a Balbiani body. *Proceedings of the National Academy of Sciences*. 104:187-192.
Pfender, S., V. Kuznetsov, M. Pasternak, T. Tischer, B. Santhanam, and M. Schuh. 2015. Live imaging RNAi screen reveals genes essential for meiosis in mammalian oocytes. *Nature*. 524:239-242.
Rao, S., G.W. Kirschen, J. Szczurkowska, A. Di Antonio, J. Wang, S. Ge, and M. Shelly. 2018. Repositioning of somatic golgi apparatus is essential for the dendritic establishment of adult-born hippocampal neurons. *Journal of Neuroscience*. 38:631-647.
Reddy, P., W. Zheng, and K. Liu. 2010. Mechanisms maintaining the dormancy and survival of mammalian primordial follicles. *Trends in Endocrinology & Metabolism*. 21:96-103.
Rimon-Dahari, N., L. Yerushalmi-Heinemann, L. Alyagor, and N. Dekel. 2016. Ovarian folliculogenesis. *In* Molecular mechanisms of cell differentiation in gonad development. Springer. 167-190.
Rinaldi, V.D., J.C. Bloom, and J.C. Schimenti. 2018. Whole mount immunofluorescence and follicle quantification of cultured mouse ovaries. *JoVE (Journal of Visualized Experiments)*:e57593.
Rugh, R. 1968. The mouse; its reproduction and development. Burgess Pub. Co.
Samaddar, M., J. Goudeau, M. Sanchez, D.H. Hall, K.A. Bohnert, M. Ingaramo, and C. Kenyon. 2021. A genetic screen identifies new steps in oocyte maturation that enhance proteostasis in the immortal germ lineage. *Elife*. 10:e62653.
Schatten, G. 1994. The centrosome and its mode of inheritance: the reduction of the centrosome during gametogenesis and its restoration during fertilization. *Developmental biology*. 165:299-335.
Shimamoto, S., Y. Nishimura, G. Nagamatsu, N. Hamada, H. Kita, O. Hikabe, N. Hamazaki, and K. Hayashi. 2019. Hypoxia induces the dormant state in oocytes through expression of Foxo3. *Proceedings of the National Academy of Sciences*. 116:12321-12326.
Sotelo, J.R. 1959. An electron microscope study on the cytoplasmic and nuclear components of rat primary oocytes. *Zeitschrift für Zellforschung und Mikroskopische Anatomie*. 50:749-765.

Tan, A., J. Bolscher, C. Feltkamp, and H. Ploegh. 1992. Retrograde transport from the Golgi region to the endoplasmic reticulum is sensitive to GTP gamma S. *The Journal of cell biology*. 116:1357-1367.
Tao, C.-C., K.-M. Cheng, Y.-L. Ma, W.-L. Hsu, Y.-C. Chen, J.-L. Fuh, W.-J. Lee, C.-C. Chao, and E.H. Lee. 2020. Galectin-3 promotes Aβ oligomerization and Aβ toxicity in a mouse model of Alzheimer's disease. *Cell Death & Differentiation*. 27:192-209.
Turner, J.R., and A.M. Tartakoff. 1989. The response of the Golgi complex to microtubule alterations: the roles of metabolic energy and membrane traffic in Golgi complex organization. *The Journal of Cell Biology*. 109:2081-2088.
Ullmann, S.L., and L. Butcher. 1996. Mammalian oocyte organelles with special reference to pleomorphic mitochondria and vacuole formation in marsupials. *Reproduction, fertility and development*. 8:491-508.
Usmani, S.M., O. Zirafi, J.A. Müller, N.L. Sandi-Monroy, J.K. Yadav, C. Meier, T. Weil, N.R. Roan, W.C. Greene, and P. Walther. 2014. Direct visualization of HIV-enhancing endogenous amyloid fibrils in human semen. *Nature communications*. 5:1-8.
van der Reest, J., G.N. Cecchino, M.C. Haigis, and P. Kordowitzki. 2021. Mitochondria: their relevance during oocyte ageing. *Ageing Research Reviews*:101378.
Wallace, W.H.B., and T.W. Kelsey. 2010. Human ovarian reserve from conception to the menopause. *PloS one*. 5:e8772.
Watanabe, T., Y. Sakai, D. Koga, H. Bochimoto, Y. Hira, M. Hosaka, and T. Ushiki. 2012. A unique ball-shaped Golgi apparatus in the rat pituitary gonadotrope: its functional implications in relation to the arrangement of the microtubule network. *Journal of Histochemistry & Cytochemistry*. 60:588-602.
Weakley, B.S. 1966. Electron microscopy of the oocyte and granulosa cells in the developing ovarian follicles of the golden hamster (Mesocricetus auratus). *Journal of anatomy*. 100:503.
Westergaard, C.G., A.G. Byskov, and C.Y. Andersen. 2007. Morphometric characteristics of the primordial to primary follicle transition in the human ovary in relation to age. *Human reproduction*. 22:2225-2231.
Wilhelm, J.E., M. Buszczak, and S. Sayles. 2005. Efficient protein trafficking requires trailer hitch, a component of a ribonucleoprotein complex localized to the ER in Drosophila. *Developmental cell*. 9:675-685.
Wischnitzer, S. 1970. An electron microscope study of cytoplasmic organelle transformations in developing mouse oocytes. *Wilhelm Roux'Archiv für Entwicklungsmechanik der Organismen*. 166:150-172.
Yang, W.-h., J.H. Yu, T. Gulick, K.D. Bloch, and D.B. Bloch. 2006. RNAassociated protein 55 (RAP55) localizes to mRNA processing bodies and stress granules. *Rna*. 12:547-554.
Zhang, Y.-Z. 1994. Novel fluorescent acidic organelle-selective dyes and mitochondrion-selective dyes that are well retained during cell fixation and permeabilization. *Mol. Biol. Cell*. 5:113a.

FIGURES

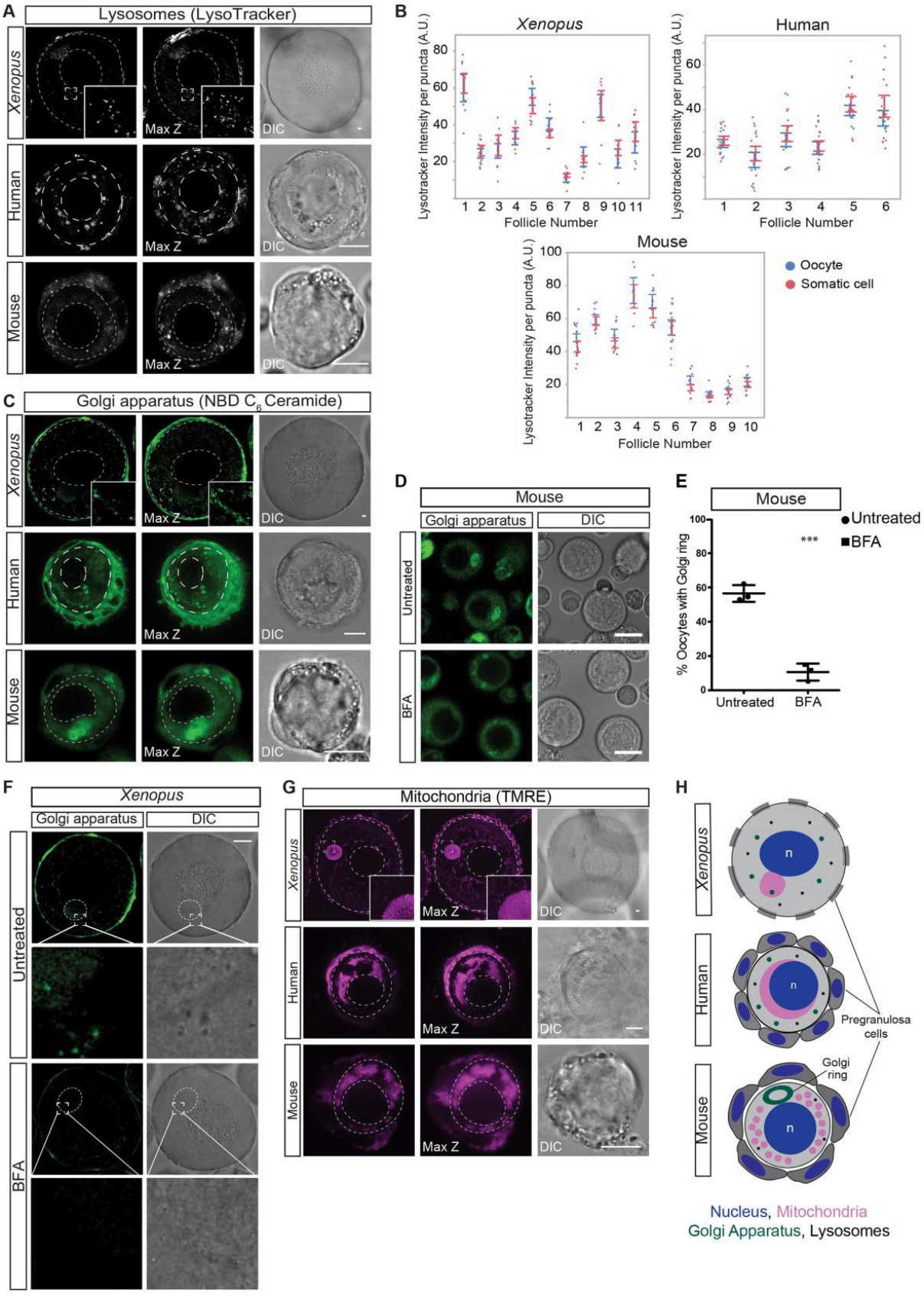
A
Lysosomes (LysoTracker)
Xenopus
Human
Mouse
Max Z
DIC
B
Xenopus
Human
Mouse
Lysotracker Intensity per puncta (A.U.)
Follicle Number
Oocyte
Somatic cell
C
Golgi apparatus (NBD C6 Ceramide)
D
Mouse
Golgi apparatus
DIC
Untreated
BFA
E
Mouse
Untreated
BFA
***
% Oocytes with Golgi ring
F
Xenopus
Golgi apparatus
DIC
Untreated
BFA
G
Mitochondria (TMRE)
H
Pregranulosa cells
Golgi ring
n
Nucleus, Mitochondria
Golgi Apparatus, Lysosomes

Fig. 1. Live-imaging of vertebrate primordial follicles reveals active organelles.
(A, C, G) Live imaging of *Xenopus*, mouse and human primordial follicles probed with **(A)** LysoTracker Deep Red to assess lysosomal activity, **(C)** NBD C_6-Ceramide to image the Golgi apparatus, and **(G)** tetramethyl rhodamine ethyl ester (TMRE) to assess mitochondrial activity. All left panels show the central plane of the oocyte. Middle panels are maximum z-projections of peri-equatorial regions and right panels are DIC images of the same oocyte. The nuclear envelope and the plasma membrane are marked with dashed circles. Insets in *Xenopus* images are 4x magnification of marked boxes. Scale bars: 10µm**.** Three individuals were examined for each species; at least 2 oocytes were imaged for each human, and at least 3 oocytes for each mouse and *Xenopus*. **(B)** Quantification of mean fluorescence intensity of LysoTracker puncta in primordial oocytes and somatic cells in the indicated species. Each dot represents a lysosome; blue and red dots represent lysosomes from oocytes and somatic cells, respectively. For each follicle, the mean fluorescence intensity of at least 3 puncta was measured on the same z-section of the oocyte and somatic cells within that follicle. Error bars represent mean ± S.E.M. **(D)** Live imaging of the Golgi apparatus in mouse primordial oocytes untreated (DMSO) or treated with Brefeldin A (BFA) and labelled with NBD C_6-Ceramide to assess trafficking of the Golgi apparatus. 3 biological replicates were performed. **(E)** Quantification of mouse oocytes containing a Golgi ring in untreated or BFA-treated oocytes from 3 biological replicates. At least 15 oocytes were counted per condition for each replicate. p-value=0.00034 was calculated with an unpaired two-tailed Student's t-test. **(F)** Live imaging of the Golgi apparatus after incubation with NBD C_6-Ceramide in *Xenopus* primordial oocytes untreated (DMSO) or treated with Brefeldin A (BFA) to assess trafficking of the Golgi apparatus. Three biological replicates were performed; more than five oocytes were imaged for each replicate. Notice the Balbiani body (dashed circle) is not disassembled by BFA treatment. Scale bar: 50µm. Insets are 4x magnification of marked boxes. **(H)** Cartoon representation of oocytes illustrating the cytoplasmic organization of organelles in *Xenopus*, human and mouse primordial oocytes. The nucleus is depicted in blue, mitochondria in magenta, the Golgi apparatus in green and lysosomes in black

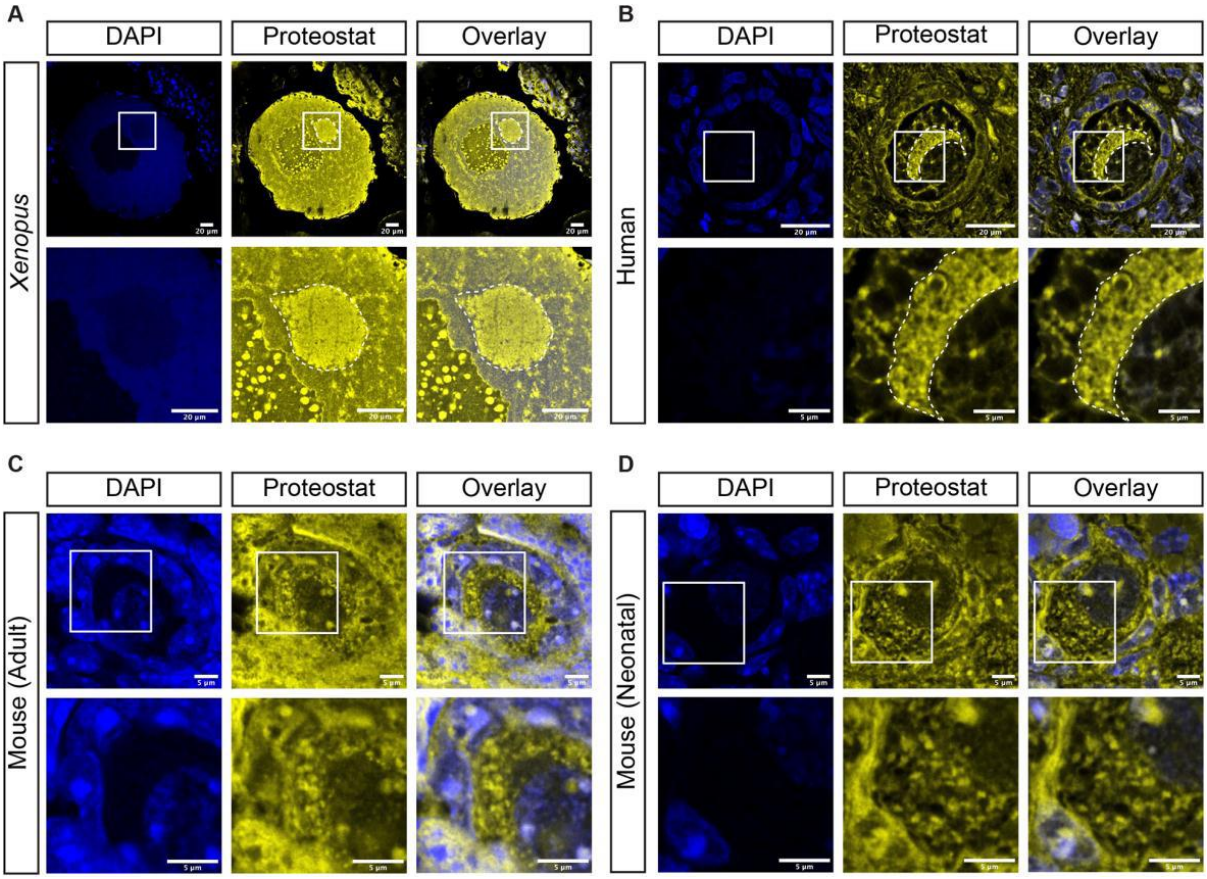

Fig. 2. Mouse primordial oocytes do not contain a large proteinaceous matrix.
Formalin-fixed paraffin-embedded sections of ovaries from **(A)** *Xenopus*, **(B)** human, **(C)** neonatal mouse (PND4) and **(D)** adult mouse (8 weeks old) were deparaffinised and labelled with Proteostat Aggresome Detection Kit to detect an amyloid-like protein matrix. Proteostat marked a structure reminiscent of the mitochondrial cluster in *Xenopus* and human oocytes, but not in mouse. Nuclei were marked with DAPI (blue). Three individuals were examined for each species; at least 3 oocytes were imaged for each human, 10 oocytes for each mouse and 5 oocytes for each *Xenopus.* Size of the scale bars are indicated in the figure.

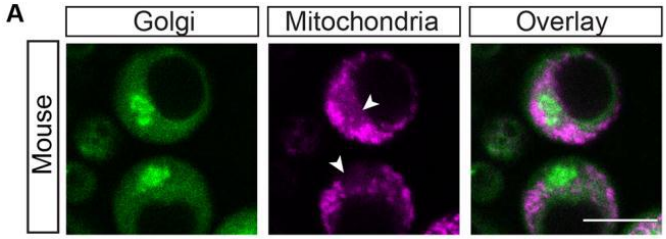

B Hypothesis 1

MEZ is maintained by the proteinaceous matrix of a Balbiani body-*like* compartment:

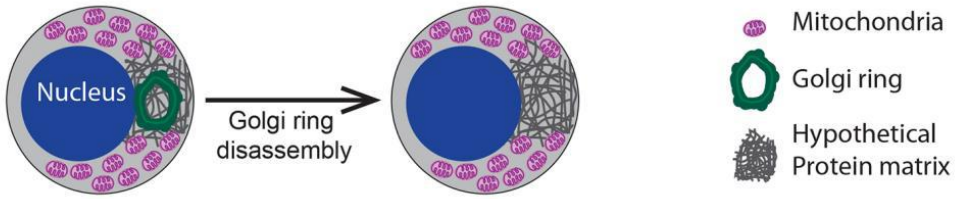

Hypothesis 2

MEZ is maintained by the Golgi ring and not a Balbiani body-*like* compartment:

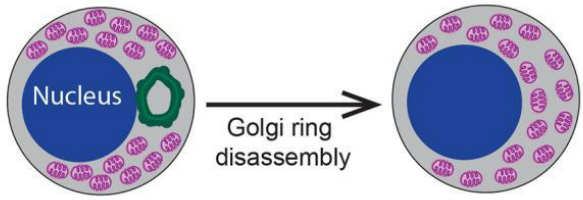

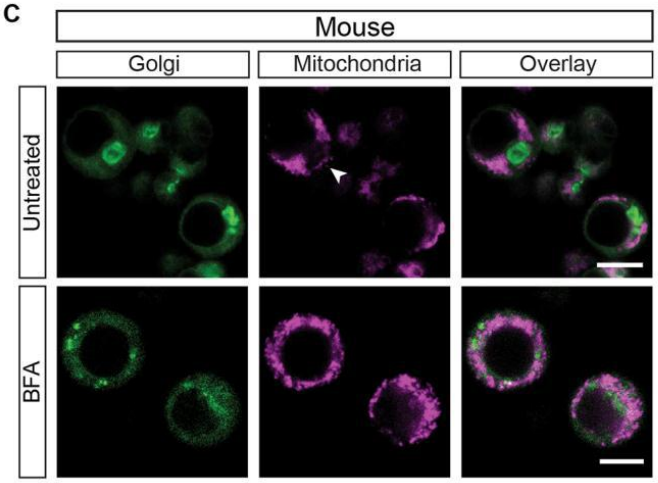

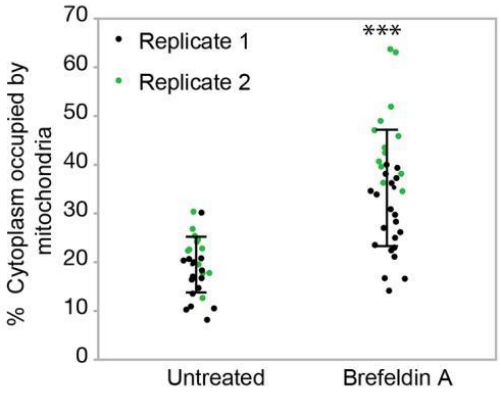

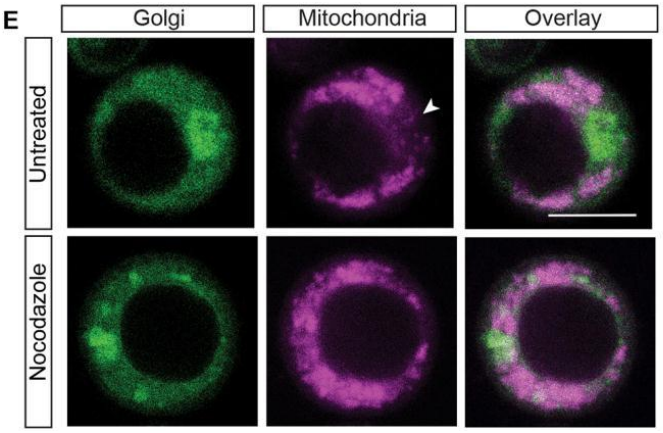

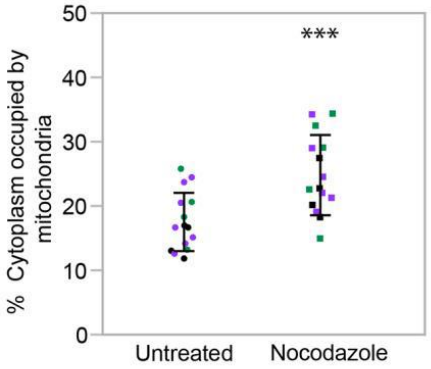

Fig. 3. The Golgi ring is not a marker for the mouse Balbiani body. (A) Simultaneous live-imaging of mitochondria and the Golgi apparatus in mouse primordial oocytes revealed a mitochondrial exclusion zone (MEZ) close to the Golgi ring. MEZ is indicated by white arrowheads. Scale bars: 10µm. **(B)** Schematic illustration of the experimental rationale for analysing mitochondrial localization after Golgi disassembly. Hypothesis 1: The Mitochondrial exclusion zone (MEZ) is maintained by the proteinaceous matrix of a Balbiani body*-like* compartment. Hence, The MEZ will be maintained after Golgi ring disassembly by Brefeldin A (BFA). Hypothesis 2: The MEZ is maintained by the Golgi ring. Hence, Golgi ring disassembly would lead to the disappearance of the MEZ as mitochondria would redistribute in the cytoplasm and the proportion of cytoplasm occupied by mitochondria would increase. Mitochondria are shown in magenta, the Golgi Ring in green and the proteinaceous matrix in dark grey. **(C)** Live-imaging of mitochondria and the Golgi apparatus in untreated or BFA-treated mouse primordial oocytes. White arrowhead indicates MEZ. Scale bars: 10µm. **(D)** Quantification of the area of oocyte cytoplasm occupied by mitochondria in untreated and BFA-treated oocytes. Each dot represents an oocyte and each colour an experiment. p-value<0.0001 calculated with a Student's t-test. Error bars indicate mean ± S.D. For (A), (C) and (D) two biological replicates from a total of 6 animals are shown. **(E)** Mouse primordial oocytes were left untreated or treated with Nocodazole to dissociate the Golgi ring, and incubated with NBD C_6-Ceramide and MitoTracker Deep Red FM. The mitochondrial exclusion zone (MEZ) is depicted by a white arrow head. Scale bars are 10µm. (**F)** Quantification of the cytoplasmic area occupied by mitochondria in untreated and Nocodazole-treated oocytes. Each dot represents an oocyte and each colour a replicate. For (E-F), n=3 biological replicates. p-value = 0.0009 was calculated with a two-tailed unpaired t-test.

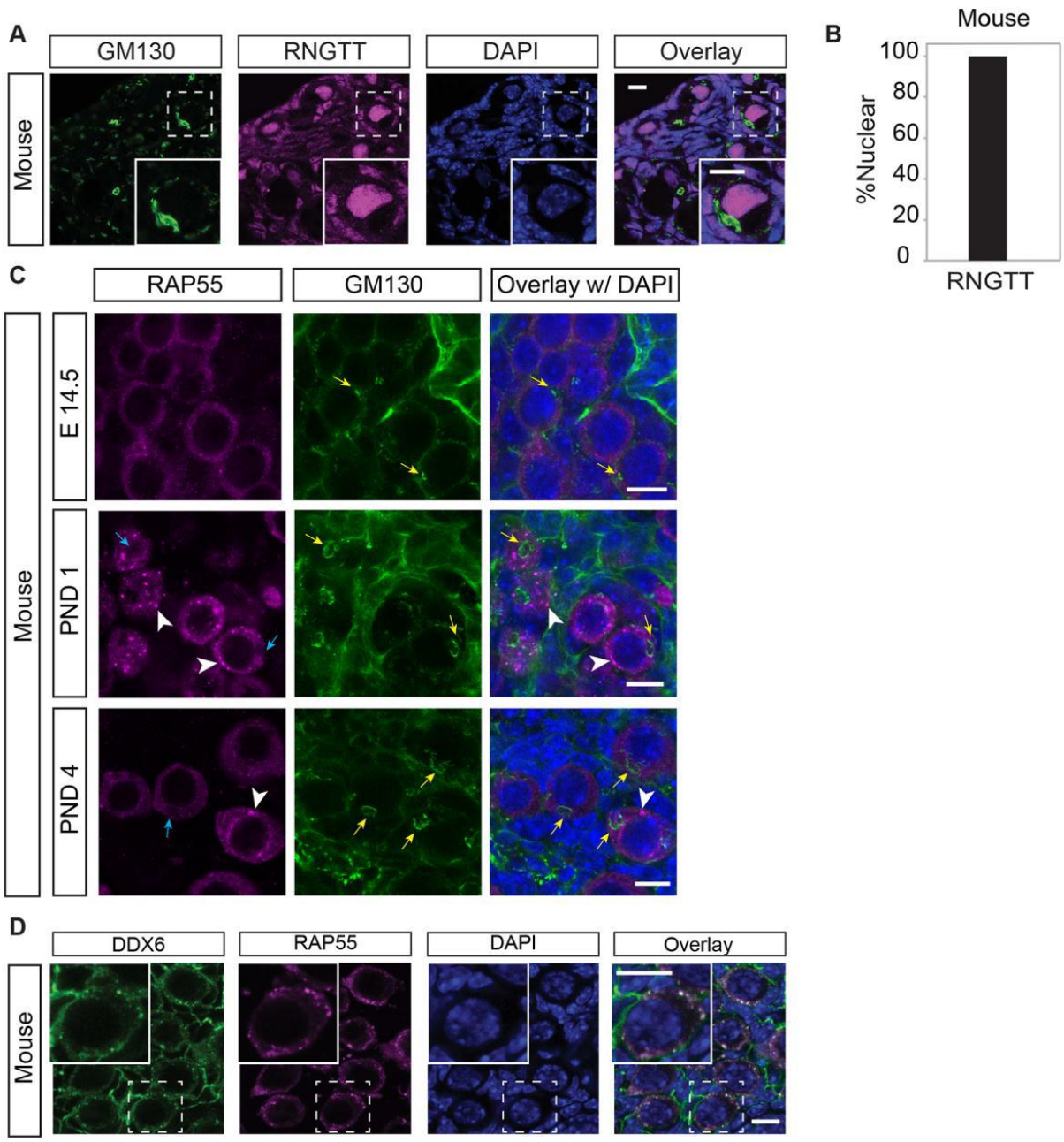

Fig. 4. The Golgi ring does not associate with the RNA-binding proteins RNGTT and RAP55. (A) Immunostaining of neonatal mouse ovary sections using antibodies against the RNA binding protein RNGTT (magenta) and the cis-Golgi marker GM130 (green). Nuclei are labelled with DAPI and are shown in blue. White dashed box depicts the area magnified in the inset. Representative images from three biological replicates are shown. **(B)** Quantification of oocytes with nuclear localization of RNGTT. At least 30 primordial oocytes were counted per replicate, 3 biological replicates were performed. All oocytes displayed nuclear RNGTT. **(C)** Whole mount immunostaining of embryonic (E14.5) and neonatal (PND1 and PND4) ovaries for RAP55 (magenta) and the cis-Golgi marker GM130 (green). The Golgi apparatus is indicated by yellow arrows. Note that in PND1 and PND4 ovaries a Golgi ring can be seen. The RAP55 granules in PND1 and PND4 are indicated by white arrow heads. RAP55 is excluded from the area of the Golgi ring (indicated by a blue arrow). n=3 for each stage. Scale bars: 10µm. Please note that some batches of mouse the monoclonal GM130 antibody stain the basal membrane in mouse ovary sections, as reported previously (Lei and Spradling, 2016). **(D)** Wholemount immunostaining of neonatal mouse ovary using antibodies against DDX6 (green) and RAP55 (magenta). Insets are 2x magnification of white dashed boxes. For

(C) and (D), three biological replicates were performed and representative images are shown. All scale bars are 10μm.

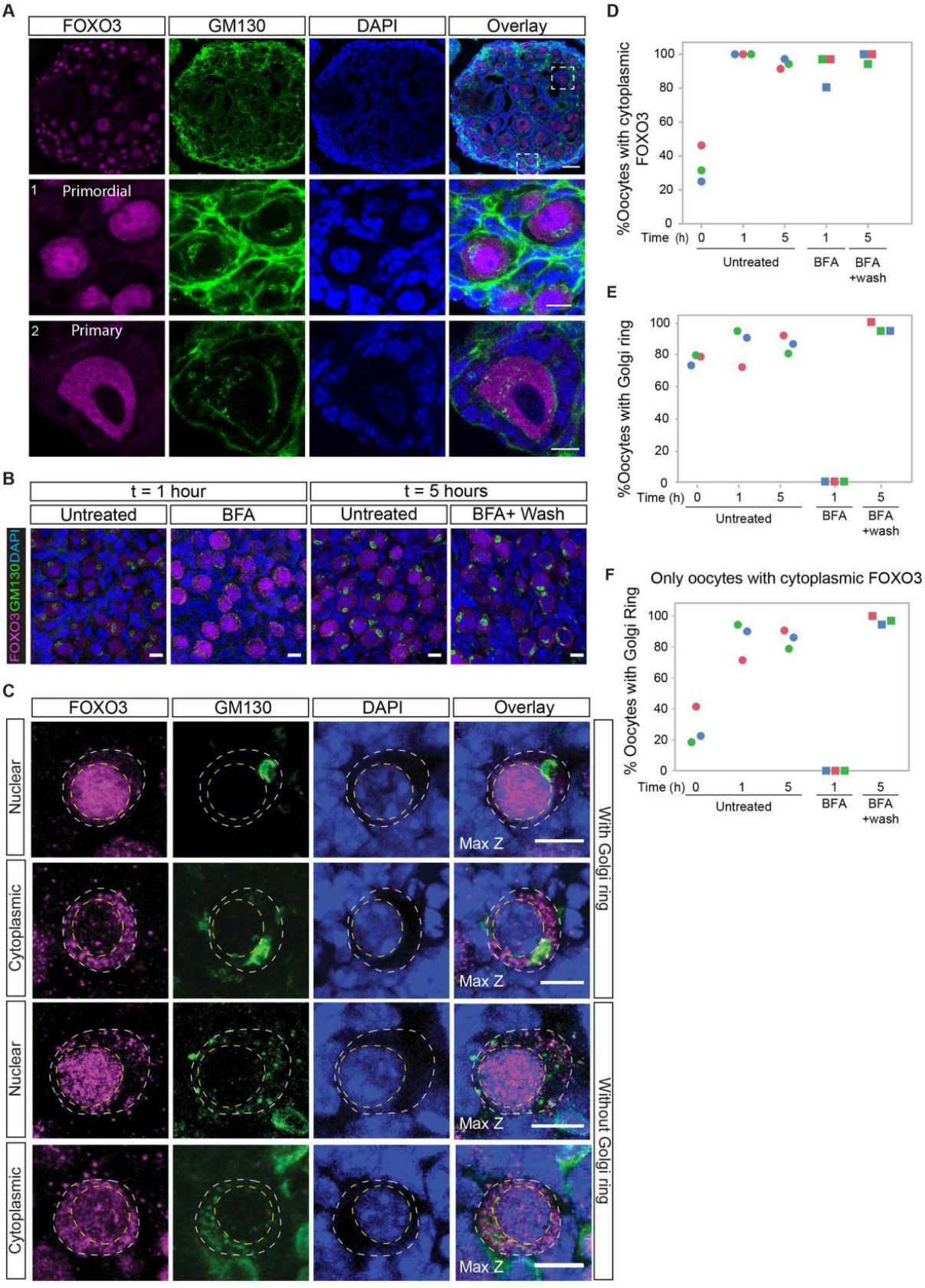

Fig. 5. The Golgi ring is not functionally associated with oocyte dormancy. (A-C) Wholemount immunostaining of neonatal mouse ovaries with FOXO3 (magenta) and GM130 (green) antibodies. **(A)** Representative image of an ovary fixed immediately after extraction. The dashed boxes indicate the areas magnified in the panels below: 1 – primordial oocytes, 2 – primary oocyte. **(B)** Representative images of ovaries that were either left untreated or treated with BFA for 1 hour *in vitro* to observe the Golgi ring disassembly (left panel) and of ovaries that were left untreated for 5 hours or treated with BFA for 1 hour followed by 4 hours of culture without BFA to observe the Golgi ring reformation (right panel). **(C)** Representative images of nuclear or cytoplasmic FOXO3 localization in oocytes with the Golgi ring (Top and Top middle, respectively), and without the Golgi ring (Bottom middle and bottom panel, respectively). Nuclei were marked by DAPI. Maximum z projections of 3 sections taken 1µm apart are shown. White dashed circles denote the oocyte membrane, yellow dashed circles the nuclear membrane. **(D-F)** Quantification of **(D)** cytoplasmic FOXO3, **(E)** the Golgi ring and **(F)** the Golgi ring in oocytes with cytoplasmic FOXO3 from wholemount images of ovaries taken at the indicated time points. Each biological replicate is represented by a different colour. Filled squares represent ovaries that were treated with BFA for 1 hour and then fixed or followed by 4 hours of culture in BFA-free medium (wash). Filled circles represent untreated ovaries at different time points. Within each of the three replicates, ovaries were taken from neonatal pups born in the same litter. Correlation analysis of FOXO3 nuclear localization and the presence of the Golgi ring between all conditions revealed no relation between the two (Linear Fit; R_2=9E-05). For (A) to (E), three biological replicates were performed. In (D) and (E), at least 30 oocytes per condition and time point were counted. All scale bars are 10µm.

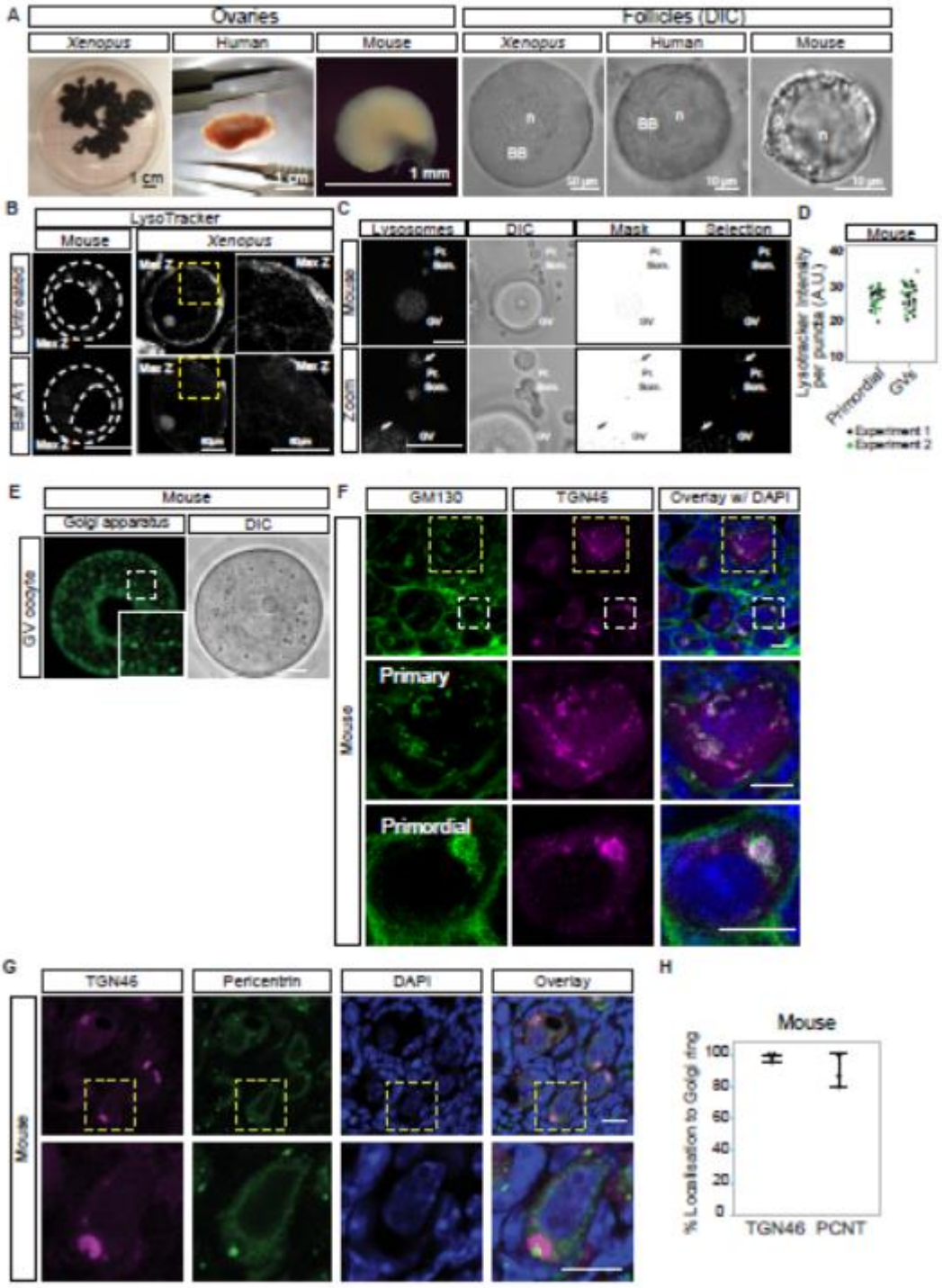

Fig. S1. Live-cell imaging reveals metabolically active lysosomes and Golgi apparatus in primordial oocytes. (A) Isolation procedure of ovarian follicles from vertebrate ovaries. Left panel: intact ovaries after dissection. Right panel: DIC microscopy images of individual ovarian follicles after isolation. All primordial oocytes have a clearly discernible nucleus (n), while the Balbiani body (BB) is visible by DIC only in *Xenopus* and human oocytes. Scale bars are as shown in each picture. **(B)** *Xenopus* and mouse primordial oocytes untreated (upper panel) or treated with Bafilomycin A1 (lower panel) to deacidify lysosomes, followed by incubation with LysoTracker. Three biological replicates were performed for each species. Scale bars: 10 µm for mouse and 60 µm for *Xenopus*. White dashed lines indicate the boundaries of oocytes and nuclei. The yellow dashed boxes indicate the areas magnified in

the adjacent panel for *Xenopus* (4X)**. (C)** Mouse primordial oocytes (Pr.), growing oocytes (GV) and ovarian somatic cells (Som.) labelled with LysoTracker. Arrows indicate LysoTracker puncta (lysosomes). Selection of puncta by creating a mask for the intensity measurement is shown. Scale bar: 25 µm. **(D)** Quantification of mean fluorescence intensity of LysoTracker puncta in mouse primordial and GV oocytes. Each dot represents a lysosome and each colour an experiment. Two biological replicates were performed using 4 neonatal (PD4) mice. p-value=not significant. **(E)** GV oocytes were imaged live after incubation with NBD C_6-Ceramide. Inset shows 2x magnification of the dashed box. Scale bars: 10 µm. Three biological replicates were performed. **(F)** Immunostaining of frozen sections of neonatal mouse ovaries (PND4) using antibodies against GM130 (green) and TGN46 (magenta). A magnification of a primordial oocyte with the Golgi ring and a primary oocyte without it (white and yellow dashed boxes, respectively) are shown in the bottom panels. Note GM130 antibody also marks the basement membrane (Lei and Spradling, 2016). Nuclei are labelled with DAPI (blue). Scale bars: 10 µm. **(G)** Immunostaining of frozen sections of neonatal mouse ovaries using antibodies against Pericentrin (green) and TGN46 (magenta). A magnification of a primordial oocyte is shown in the bottom panel. Nuclei are labelled with DAPI (blue). Scale bars: 10 µm. **(H)** Quantification of tissue sections as shown in B and C to score the percentage of oocytes in which TGN46 and pericentrin localize to the Golgi ring. At least 30 primordial oocytes were counted per replicate, 3 biological replicates were performed. Error bars represent mean ± S.D.

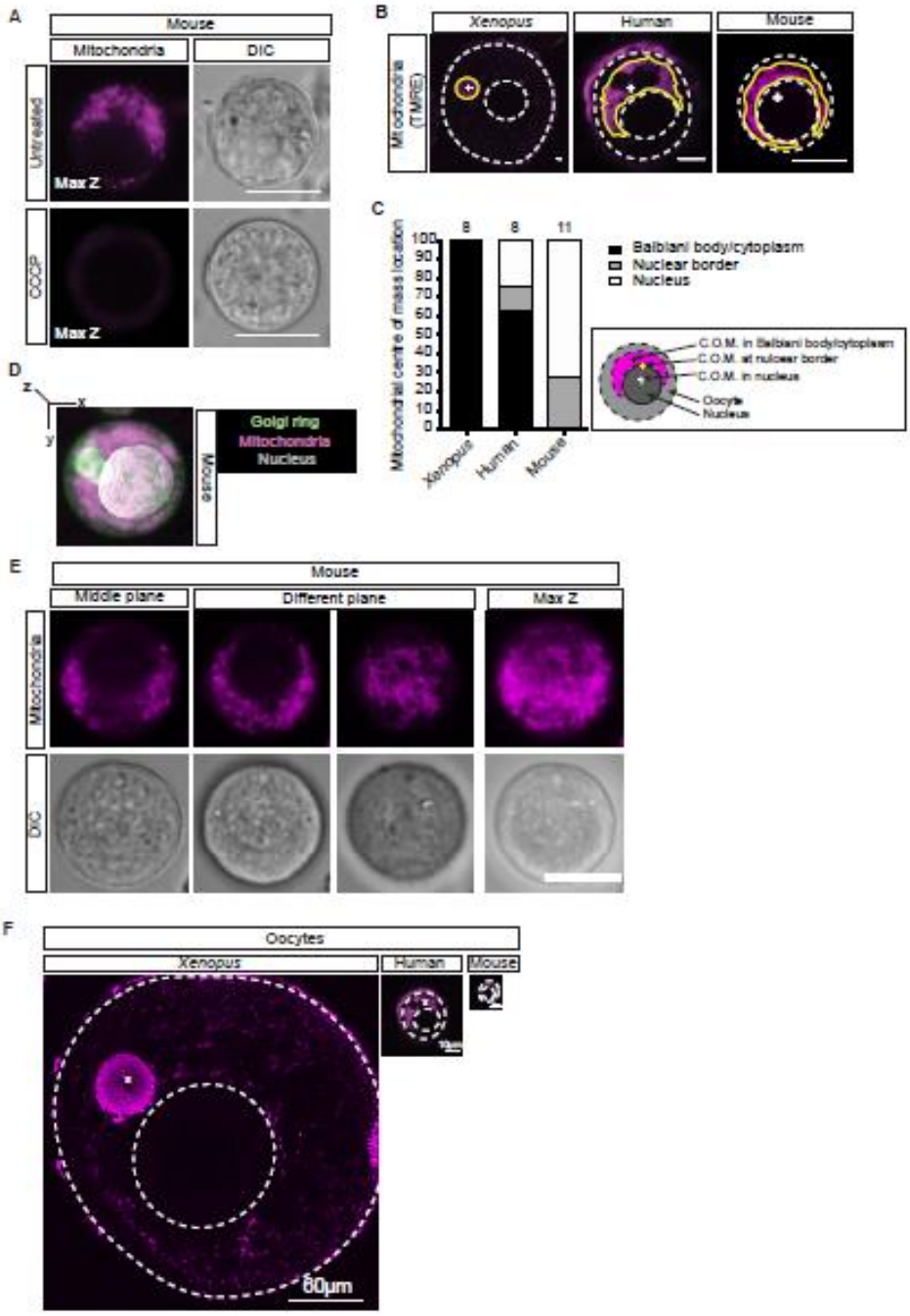

Fig. S2. Live-cell imaging of mouse primordial oocytes reveals metabolically active mitochondria dispersed throughout their cytoplasm. (A) Mouse primordial oocytes were treated with CCCP to dissipate mitochondrial membrane potential, followed by incubation with TMRE to image mitochondria. Two biological replicates were performed using a total of 4 mice. **(B, C)** Calculation of the center of mass (C.O.M.) of the mitochondrial distribution in *Xenopus*, human and mouse primordial oocytes. Yellow outline indicates the delineation of the mitochondrial mass, the white "+" symbol indicates the location of the C.O.M. in each species while white dashed line marks the outline of the oocyte and nucleus. Scale bar: 10 µm. The number of oocytes of each species used in the quantification is indicated above each bar in the graph. **(D)** 3D reconstruction of a mouse primordial oocyte incubated with MitoTracker Deep Red FM to label mitochondria (magenta) and NBD C_6-Ceramide to label the Golgi apparatus (green). Mitochondria are distributed throughout the oocyte cytoplasm. Nucleus is depicted in white. **(E)** A mouse primordial oocyte incubated with TMRE to label

mitochondria was imaged through its volume and different z-sections are represented. Mitochondria display a dispersed distribution away from the mid plane. Scale bar: 10 µm. Three biological replicates were performed using a total of 6 mice. **(F)** Size comparison of primordial oocytes of *Xenopus*, human and mouse after incubation with TMRE. Scale bar for *Xenopus*: 60 µm, human: 10 µm and mouse: 10 µm. Gaps within the mitochondrial conglomeration in the *Xenopus* and human Balbiani body are marked by a white asterisk (*). Mitochondria are labelled with TMRE. Scale bars are as indicated in the figure.

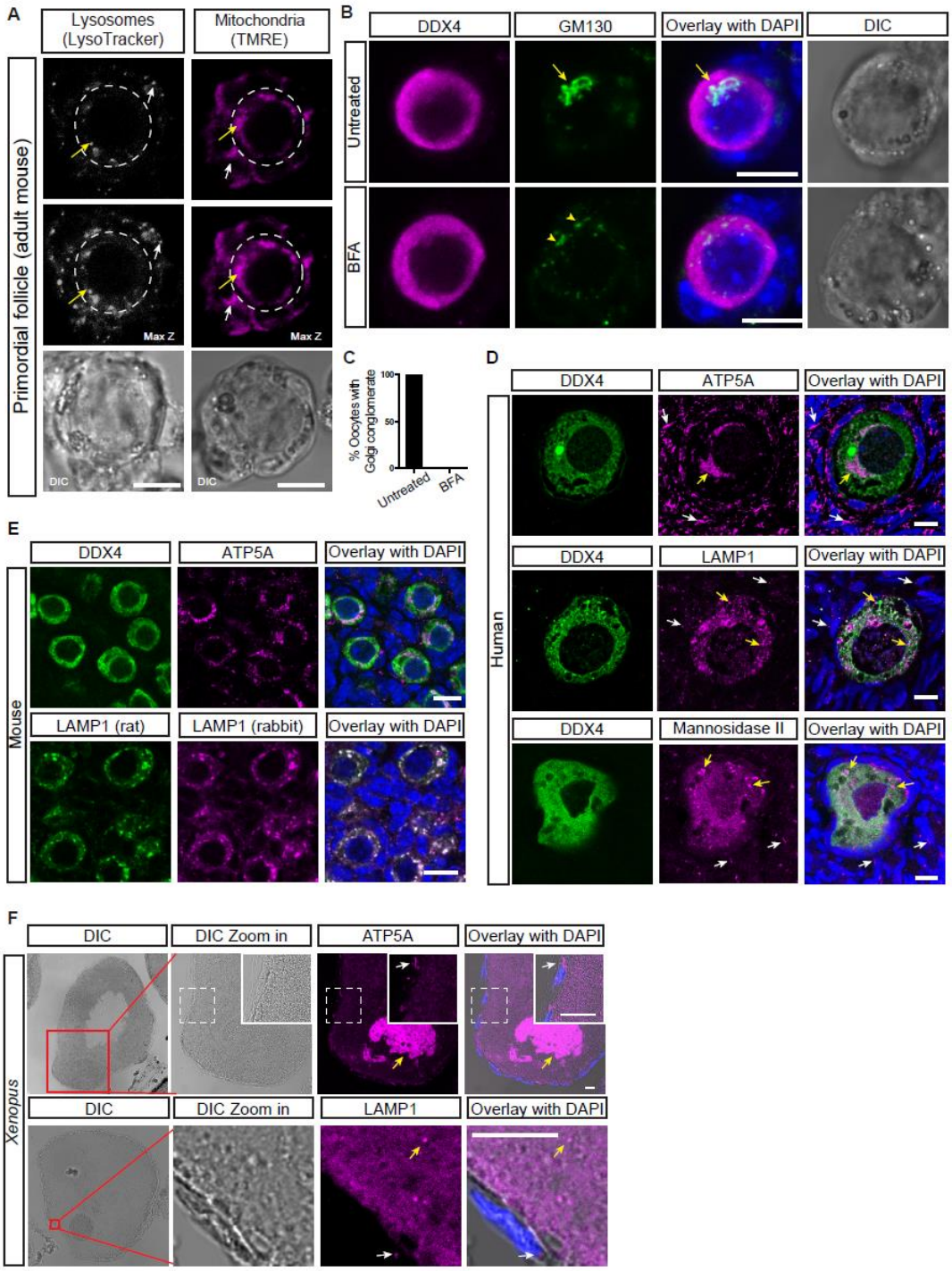

Fig. S3. Immunofluorescence of the distribution of organelles in *Xenopus*, human and mouse primordial oocytes confirms the patterns observed by live-cell imaging. (A) Live-imaging of primordial follicles isolated from young adult mice probed with LysoTracker Deep Red to assess lysosomal activity (left panel), and tetramethyl rhodamine ethyl ester (TMRE) to assess mitochondrial activity (right panel). White arrows depict lysosomes/ mitochondria in somatic cells, and yellow arrows in oocytes. While dashed lines indicate the oocyte boundary. Scale bars: 10 µm. Two biological replicates were performed; at least 4 oocytes per replicate were imaged. **(B)** Immunostaining of primordial oocytes isolated from young adult mice to detect Golgi apparatus. Oocytes were treated with BFA for 30 minutes, or left untreated (DMSO). The oocyte marker DDX4 is shown in magenta and the cis-Golgi protein GM130 in green. Nuclei are marked with DAPI (blue). The Golgi conglomerate in the untreated oocyte is indicated by the yellow arrow. The Golgi apparatus is fragmented upon BFA treatment and the fragments are represented by yellow arrow heads. Scale bars: 10 µm. **(C)** Quantification of **(B)**. A total of 6 mice were used and 17 primordial follicles were imaged. **(D)** Top, middle: paraffin-embedded sections of human ovaries were labelled with antibodies against the mitochondrial protein ATP5A (top, magenta), the lysosomal protein LAMP1 (middle, magenta), along with the oocyte-specific marker DDX4 (green). Bottom: Frozen sections of human ovaries were labelled with cis-Golgi marker, Mannosidase II (magenta) along with the oocyte specific marker DDX4 (green). Nuclei were marked with DAPI (blue). Yellow arrows point to oocyte mitochondria, lysosome or Golgi apparatus respectively while white arrows indicate their somatic cell counterparts. We sometimes observe DDX4 (shown in figure) and LAMP1 (not shown) accumulation in the mid-section of the human Balbiani Body, which correspond to the vesicular aggregates reported in the literature (Adams & Hertig, 1967). For all panels, representative images from at least 2 individuals are shown. The gaps in the oocyte cytoplasm observed by the cytoplasmic DDX4 signal arise from the fixation and processing steps during which the relatively large and spherical oocytes undergo cytoplasmic rupture. Since Golgi apparatus in human primordial oocytes have not been imaged by immunofluorescence techniques before, we used three different Golgi markers: two cis-Golgi markers (GM130 and Mannosidase II), and one trans-Golgi marker (TGN46). A similar pattern of Golgi staining (dispersed Golgi apparatus and no conglomeration) was observed with all three antibodies. Moreover, the juxtanuclear location of Golgi apparatus in somatic cells further confirmed the specificity of these Golgi markers. Here a representative image of one of the cis-Golgi markers (Mannosidase II) is shown. Scale bars: 10 µm. **(E)** Paraffin-embedded sections of ovaries from neonatal mouse (PND4) were labelled with antibodies against the mitochondrial protein ATP5A and the oocyte-specific marker DDX4 (top), or with two antibodies against the lysosomal protein LAMP1 (bottom). Nuclei were marked with DAPI (blue); n=3. **(F)** Paraffin-embedded sections of ovaries from *Xenopus* were labelled with antibodies against the mitochondrial protein ATP5A (top), or the lysosomal protein LAMP1 (bottom). Nuclei were marked with DAPI (blue). Red box in the DIC indicates the magnified area shown on the side. White dashed boxes denote the magnified areas shown in the insets. The white arrow points to the mitochondria or a lysosome in a somatic cell. The yellow arrow indicates the mitochondria in the Balbiani body or a lysosome within the oocyte. Representative images from 3 biological replicates are shown. Immunostaining of the Golgi apparatus in *Xenopus* sections could not be provided since none of the Golgi antibodies we tried worked on *Xenopus* sections. All scale bars are 10 µm.

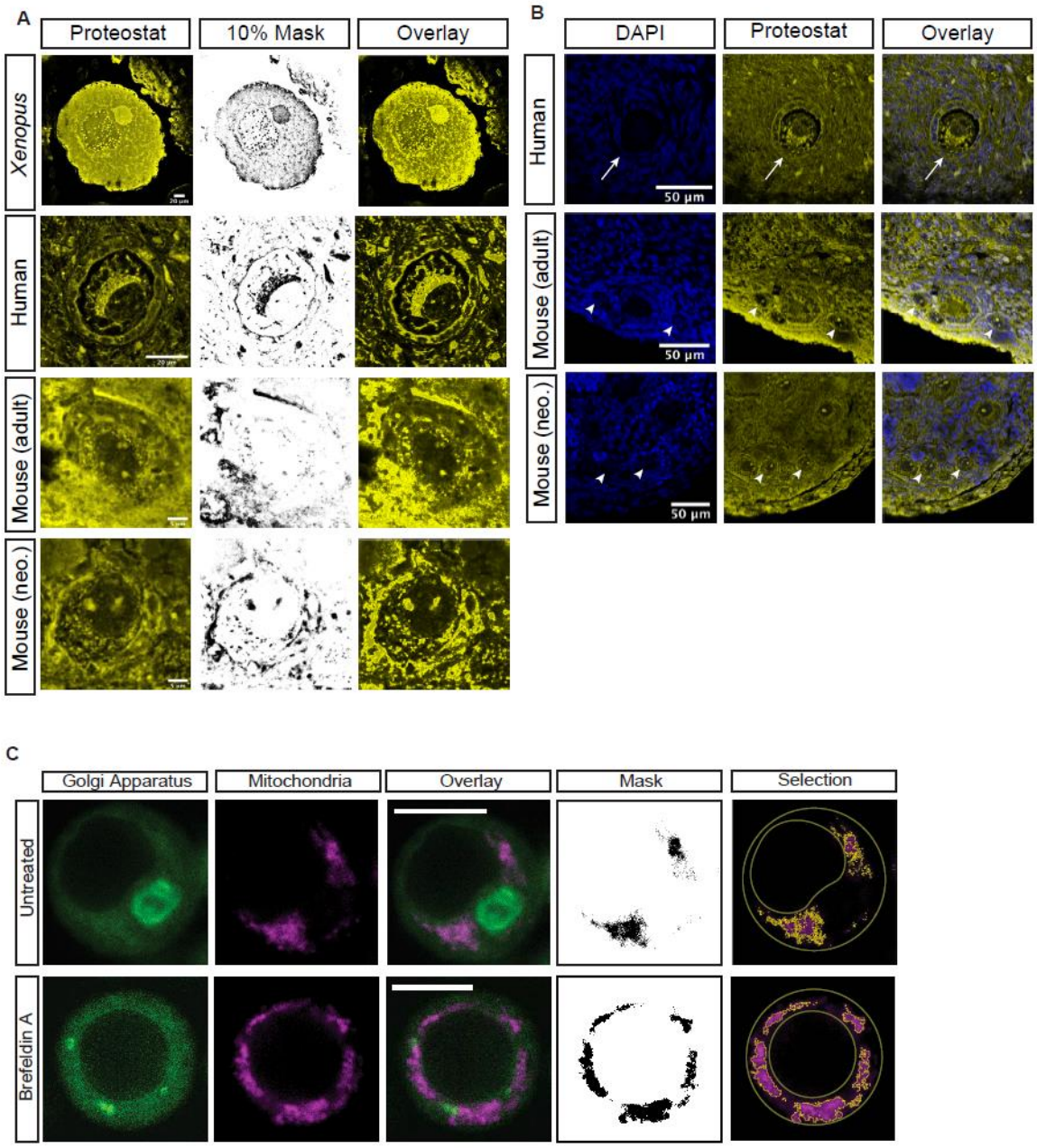

Fig. S4. The Proteostat dye marks a proteinaceous matrix in *Xenopus* and human, but not in mouse oocytes (A) Proteostat-labelled sections of *Xenopus*, human and mouse ovaries from Figure 2 are shown with fluorescent intensity masks. When thresholding masks were created to mark the top 10% fluorescence intensity in these images, the Balbiani body in *Xenopus* and human oocytes became apparent while only diffuse granules were apparent in the cytoplasm of mouse oocytes. Nucleoli, which are phase separated compartments and contain amyloid-like material in *Xenopus* oocytes (Banani et al., 2017; Hayes and Weeks, 2016) were marked with Proteostat in all three species. **(B)** Low magnification images of human and mouse ovaries labelled with Proteostat are shown. The human Balbiani body stands out in the image whereas in mouse ovaries, only nucleoli are apparent. A human primordial oocyte is marked by a white arrow while mouse primordial oocytes are marked by white arrowheads. As in Figure 2, three individuals were examined for each species;

at least 3 oocytes were imaged for each human, 10 oocytes for each mouse. **(C)** Quantification strategy to assess cytoplasmic occupancy of mitochondria after Golgi dissociation. Mitochondrial occupation of the cytoplasm was calculated dividing the area occupied by mitochondria by the cytoplasmic area. Scale bars: 10 μm.

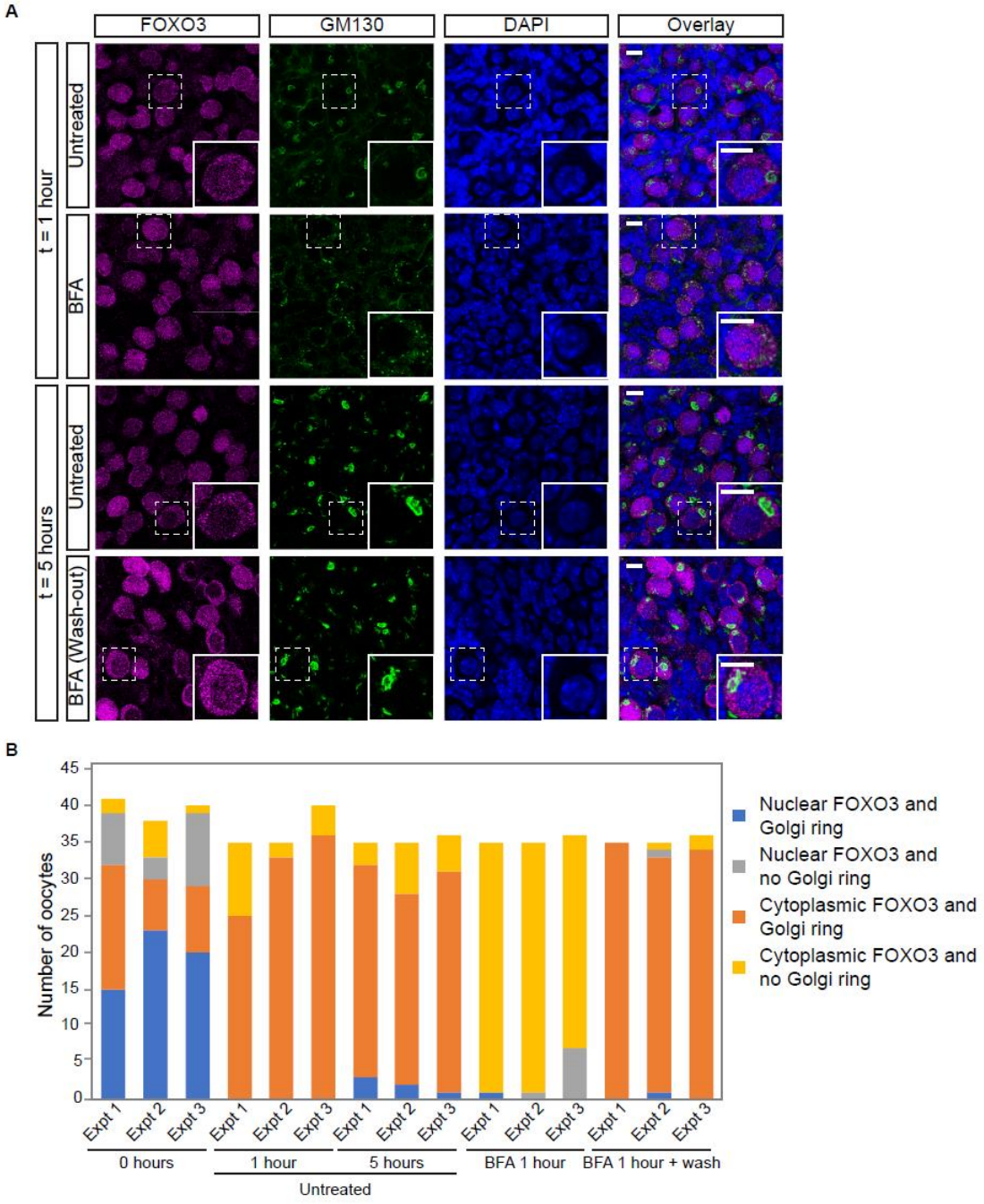

Fig. S5. Golgi ring assembly and FOXO3 localization in BFA-treated ovaries. (A) Representative images of ovaries that were either left untreated or treated with BFA for 1 hour in vitro to observe the Golgi ring disassembly (top panel) and of ovaries that were left untreated for 5 hours or treated with BFA for 1 hour followed by 4 hours of culture without BFA to observe the Golgi ring reformation (bottom panel). Shown are split-channel views and magnifications of the overlays shown in Fig. 5B. Dashed boxes

indicate the areas magnified in the insets. Scale bars: 10 µm. **(B)** Quantification of oocytes with nuclear or non-nuclear FOXO3 localization scored for the presence or absence of a Golgi ring from wholemount immunostaining images shown in Fig. 5 at the indicated time points. Three biological replicates were performed, at least 30 oocytes per condition and time point were counted.

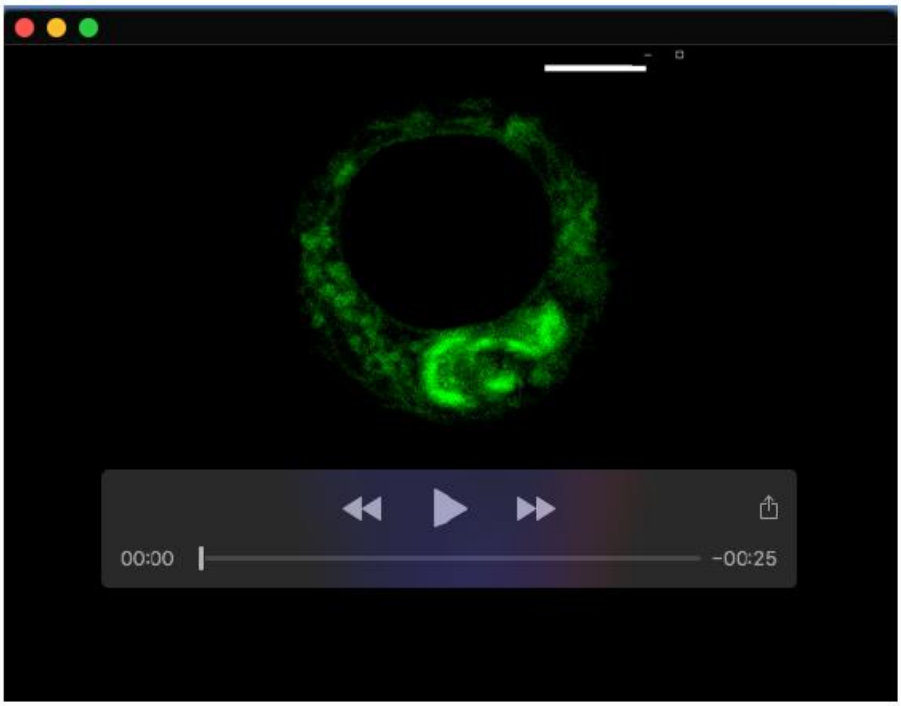

Movie 1. The Golgi ring in mouse primordial oocytes. Live-cell imaging of a mouse primordial oocyte incubated with NBD C_6-Ceramide to image the Golgi apparatus. Images of the oocyte were acquired at 10 second intervals for a total time of 3 minutes. The drift was corrected using the StackReg plugin in Fiji/ImageJ. The movie is played at 5 frames/second. Scale bar: 5 µm.

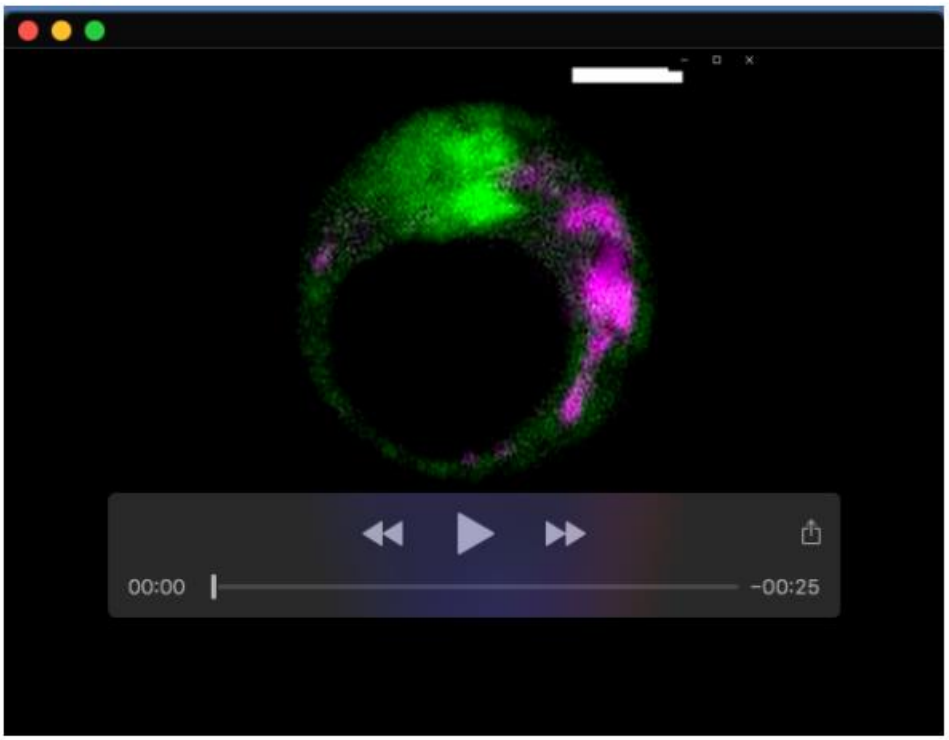

Movie 2. Mitochondria and Golgi ring of mouse primordial oocytes are spatially segregated. Live-cell imaging of a mouse primordial oocyte incubated with NBD C_6-Ceramide and MitoTracker Deep Red FM to image the Golgi apparatus and mitochondria, respectively. Images acquired at 30 second intervals for a total time of 5 minutes. The drift was corrected using the StackReg plugin in Fiji/ImageJ. The movie is played at 1 frame/second. Scale bar: 5 μm

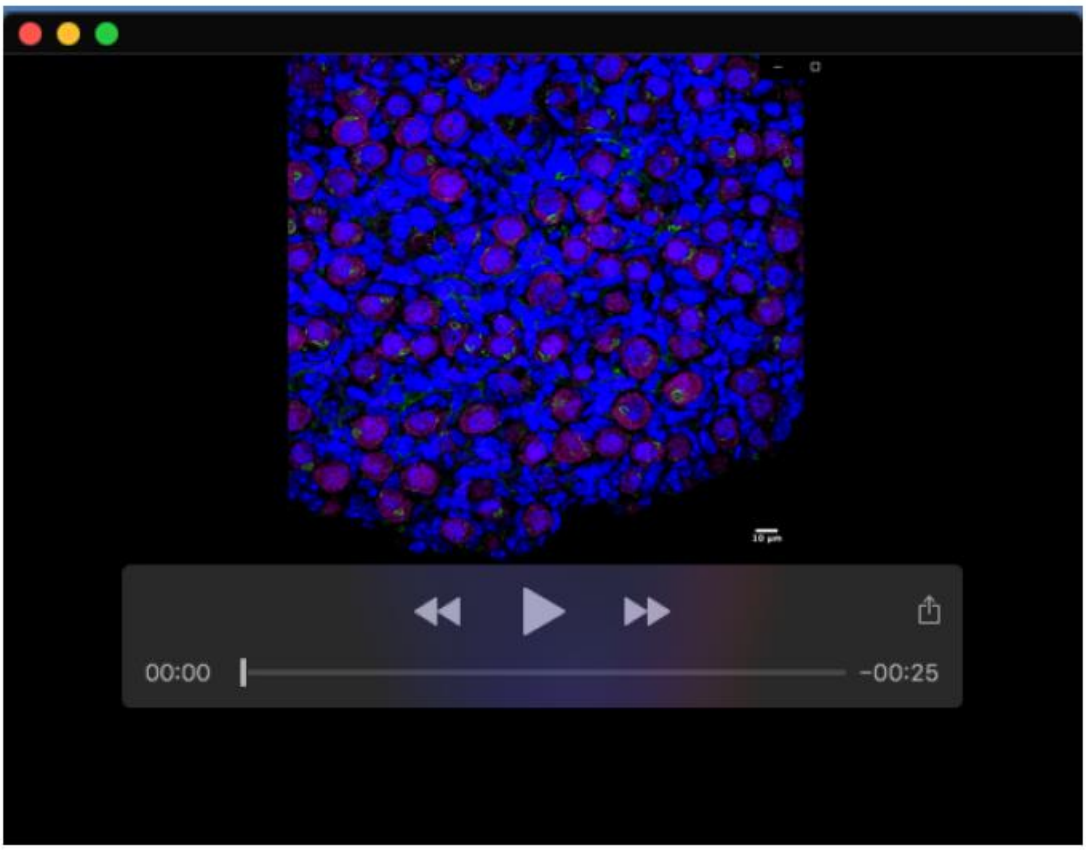

Movie 3. Z-stack images of a representative untreated ovary shown in Fig. 5B-F. Whole mount immunostaining of a neonatal ovary with FOXO3 (magenta) and GM130 (green) antibodies after 1 hour in vitro culture. Scale bar: 10 µm

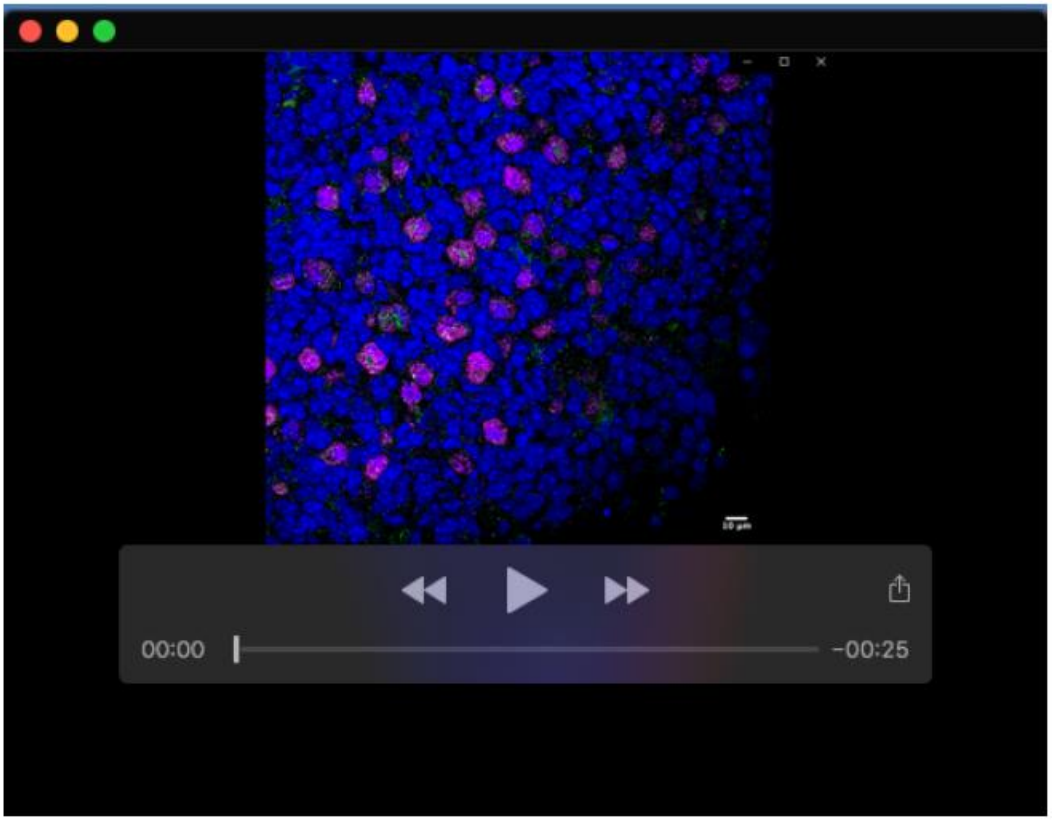

Movie 4. Z-stack images of a representative ovary shown in Fig. 5B-F after Brefeldin A (BFA) treatment. Wholemount immunostaining of a neonatal ovary with FOXO3 (magenta) and GM130 (green) antibodies after 1 hour in vitro culture in the presence of BFA. Scale bar: 10 µm.

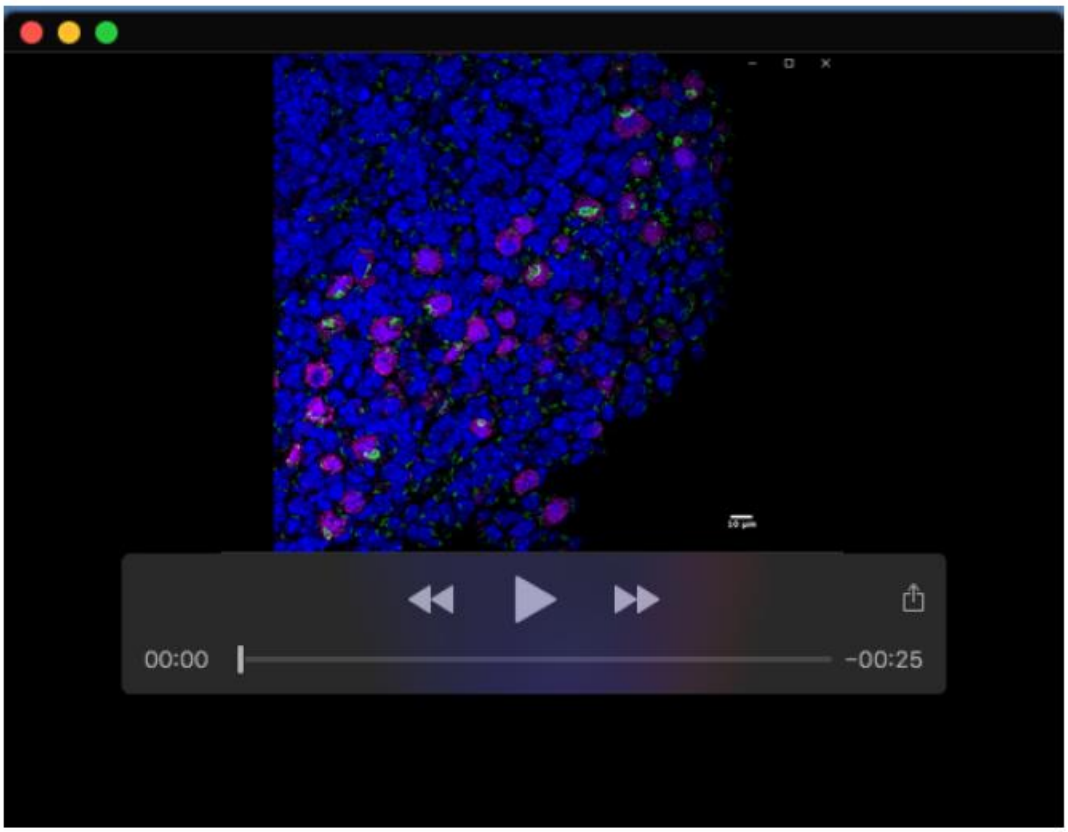

Movie 5. Z-stack images of a representative untreated ovary shown in Fig. 5B-F after 5 hours of in vitro culture. Whole-mount immunostaining of a neonatal ovary with FOXO3 (magenta) and GM130 (green) antibodies after 5 hours in vitro culture. Scale bar: 10 µm.

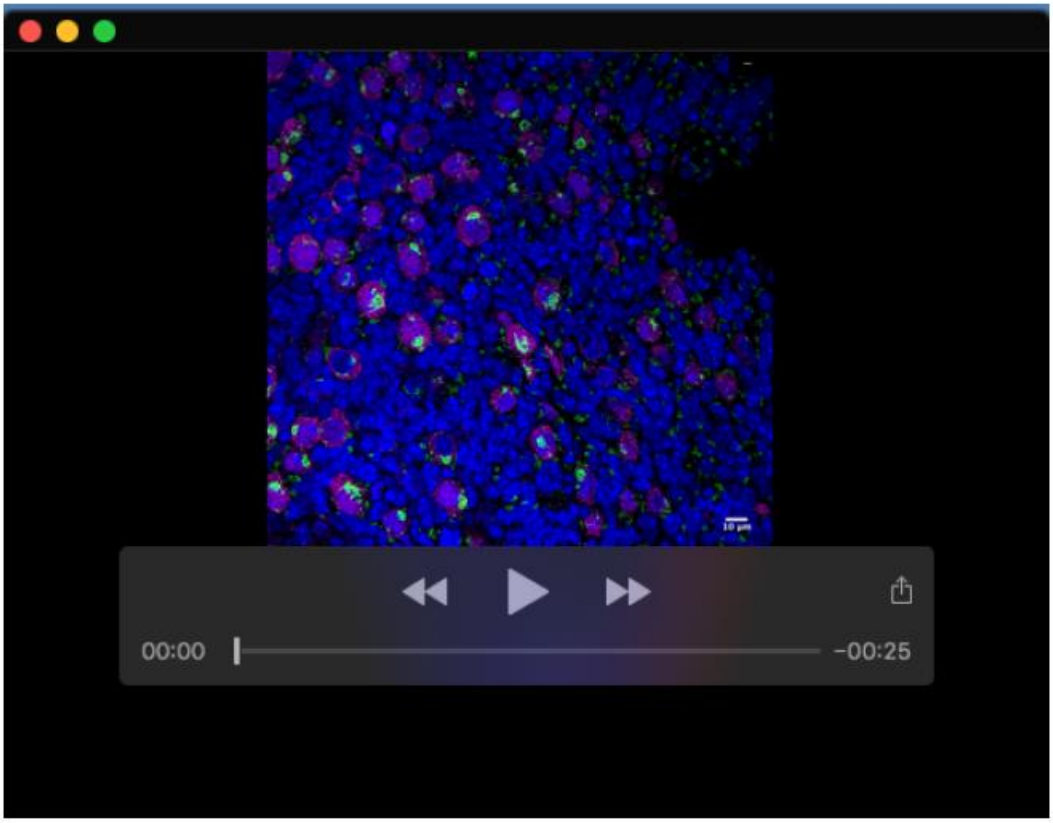

Movie 6. Z-stack images of a representative ovary shown in Fig. 5B-F after BFA treatment followed by wash-out. Whole-mount immunostaining of a neonatal ovary with FOXO3 (magenta) and GM130 (green) antibodies after treatment with BFA for 1 hour and followed by incubation for 4 hours in a BFA-free medium. Scale bar: 10 μm.